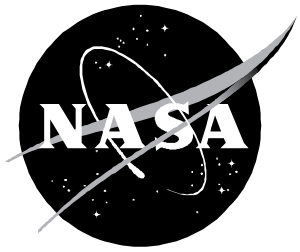

NASA Technical Paper 3641
ARL Technical Report 1279

Stiffness Characteristics of Composite Rotor Blades With Elastic Couplings

David J. Piatak
Langley Research Center • Hampton, Virginia

Mark W. Nixon
Vehicle Structures Directorate
U.S. Army Research Laboratory
Langley Research Center • Hampton, Virginia

John B. Kosmatka
Department of Applied Mechanics in Engineering Science
University of California • San Diego, California

National Aeronautics and Space Administration
Langley Research Center • Hampton, Virginia 23681-0001

April 1997

Available electronically at the following URL address: http://techreports.larc.nasa.gov/ltrs/ltrs.html

Printed copies available from the following:

NASA Center for AeroSpace Information
800 Elkridge Landing Road
Linthicum Heights, MD 21090-2934
(301) 621-0390

National Technical Information Service (NTIS)
5285 Port Royal Road
Springfield, VA 22161-2171
(703) 487-4650

Abstract

Recent studies on rotor aeroelastic response and stability have shown the beneficial effects of incorporating elastic couplings in composite rotor blades. However, none of these studies have clearly identified elastic coupling limits and the effects of elastic couplings on classical beam stiffnesses of representative rotor blades. Knowledge of these limits and effects would greatly enhance future aeroelastic studies involving composite rotor blades. The present study addresses these voids and provides a preliminary design database for investigators who may wish to study the effects of elastic couplings on representative blade designs. The results of the present study should provide a basis for estimating the potential benefits associated with incorporating elastic couplings without the need for first designing a blade cross section and then performing a cross-section analysis to obtain the required beam section properties as is customary in the usual one-dimensional beam-type approach.

Introduction

Composite materials have been used extensively in the construction of modern rotor blades for helicopters and are to be used in the blades of the V-22 tilt-rotor aircraft. These materials possess higher strength-to-weight ratios than metals and have resulted in blades which can outlast the life of the airframe because of their long fatigue life and high corrosion resistance. Desirable characteristics such as these lead to a more structurally reliable blade. For the aeroelastic and aeromechanical stability of rotor systems, elastic tailoring of composite rotor blades through specialized design of composite laminates has been a prevalent research topic. Although elastic tailoring has not yet been fully used in the design of modern composite rotor blades, it is recognized that elastic tailoring has the potential of significantly improving the aeroelastic performance of rotorcraft equipped with such blades over those equipped with conventional state-of-the-art metal or composite blades. For this reason, elastic tailoring of composite rotor blades through the specialized design of composite laminates has been a popular research topic in recent years.

Kinematic couplings have been used as a basic design tool to improve the aeroelastic and aeromechanical stability of conventional metal and composite rotor blades. However, elastic tailoring of composite blades can be used to introduce such couplings more efficiently than in metal blades and in configurations where kinematic couplings are not feasible. The first pioneering efforts to address the impact of elastically coupled composite rotor blades on rotorcraft performance and stability were begun by Hong and Chopra, references 1, 2, and 3. Although these studies used a simple composite beam analysis combined with a spanwise finite-element discretization of the blade, the potential of elastically tailored composite rotors was demonstrated for hingeless and bearingless rotors in hover. The previous work of Hong and Chopra was continued by Panda and Chopra in reference 4 by examining the dynamics of composite rotors in forward flight. The effects of ply orientation of composite lamina and elastic couplings on vibration levels and isolated rotor stability in forward flight were determined in this work. Ormiston, references 5 and 6, demonstrated that pitch-lag and flap-lag structural coupling can be very useful in avoiding both air and ground resonance in soft in-plane hingeless rotors. Without such aeroelastic couplings, weight-increasing elastomeric dampers must be included in the rotor design to increase the lead-lag damping and therefore avoid air and ground resonance. The use of elastically coupled composite rotor blades to reduce vibration and improve aeroelastic and aeromechanical stability characteristics of hingeless rotor helicopters was addressed in reference 7. This research has shown that the use of negative pitch-lag elastic coupling results in up to a 300-percent increase in lag-mode damping compared to a blade without elastic coupling. Elastic couplings were shown to have a significant influence on ground and air resonance. For example, the use of negative pitch-lag elastic coupling increased the regressive lag-mode damping in air resonance conditions but greatly decreased damping for ground resonance stability. Other couplings were found to destabilize the system in the ground resonance condition. The effect of elastically coupled rotor blades on the aeroelastic stability of tilt-rotor aircraft was investigated in reference 8. The use of

flapwise-bending-twist-coupled rotor blades was determined to have a strong stabilizing influence on the tilt-rotor whirl-flutter phenomenon which is associated with the high-speed airplane mode of flight which exhibits a 44-percent increase in flutter velocity by using only a very moderate amount of coupling. This increased flutter stability was attained without creating adverse effects on rotor performance or blade loads. The potential for improved hover performance by using extension-twist-coupled blades was also considered in the study.

While past studies have shown the benefits associated with the use of elastic couplings on rotor aeroelastic response and stability, these studies have not clearly defined elastic-coupling limits and the effects of elastic couplings on classical beam stiffnesses of representative rotor blades. A knowledge of these limits and effects would greatly enhance future aeroelastic studies involving composite blades. The present study addresses these voids and attempts to provide a preliminary design database for investigators who may wish to study the effects of elastic couplings on the classical beam stiffnesses that have been used in blade designs. The results of the present study should provide a basis for estimating the potential benefits associated with incorporating elastic couplings without the need for first designing detailed blade cross sections and then performing cross-section analyses to obtain the required one-dimensional beam section properties which are used in design.

This paper has two main objectives. The first is to determine the physical limits of several possible types of elastic couplings and to examine the effects of these elastic couplings on the stiffness characteristics of composite rotor blades over a wide range of blade-design parameters. The second objective is to present the results of this parametric study in a graphical form useful to a designer. The blade properties that varied in the parametric studies include section chord, width of spar, ply orientation angle, ratio of plies contributing to coupling, and material. The changes in the blade cross-section values of EI and GJ associated with the parametric variations are compared to two baseline designs which were defined as representative of composite rotor blades. Both baseline designs employ an NACA 0012 airfoil, a D-spar, and an internal core material aft of the D-spar. The parametric studies were performed by using a recently developed finite-element-based composite blade cross-section analysis (ref. 9) that includes the effects of cross-section in-plane and out-of-plane warping on the stiffness properties of the blade.

Symbols

c	chord, in.
EI_f	flapwise flexural stiffness, lb-in^2
EI_c	chordwise flexural stiffness, lb-in^2
GJ	torsional stiffness, lb-in^2
k_{14}	extension-twist stiffness, lb-in.
k_{24}	flapwise-bending-twist stiffness, lb-in^2
k_{34}	chordwise-bending-twist stiffness, lb-in^2
M_η, M_ζ	bending moments
M_z	torsional moment
P	tensile force
t_{sk}	skin thickness, nondimensionalized by chord
t_{sp}	spar thickness, nondimensionalized by chord
w_s	spar widths, nondimensionalized by chord
β_{EI_f}	flapwise flexural stiffness ratio
β_{EI_c}	chordwise flexural stiffness ratio
β_{GJ}	torsional stiffness ratio
δ	number of chordwise divisions within airfoil cross section
ζ_θ	fraction of plies in layup contributing to elastic coupling; off-axis plies
ζ_{45}	fraction of $\pm 45°$ plies
ζ_0	fraction of $0°$ plies
θ	ply orientation angle of cloth material, deg; blade twist rate
Ψ_{CT}	nondimensional chordwise-bending-twist coupling parameter
Ψ_{ET}	nondimensional extension-twist coupling parameter
Ψ_{FT}	nondimensional flapwise-bending-twist coupling parameter
$(\ )_{\mathrm{sk}}$	value associated with skin
$(\ )_{\mathrm{sp}}$	value associated with spar
$(\ )_o$	value associated with elastically uncoupled blade

Mechanics of Composite Blades With Elastic Couplings

The anisotropic characteristics of composites allow the design of laminates for composite blades that

exhibit the desired type of elastic couplings to be designed into rotor blades. Generally, there are several plies containing long fibers embedded in an epoxy resin matrix within each laminate of a composite blade. These fibers provide the directional nature of the laminate's stiffness and can be oriented at an angle that is off-axis from that of the principal axis of the blade, thus introducing elastic couplings into the rotor blade.

For practical purposes, it is assumed that effects of hygrothermal warping (coupling associated with thermal and moisture effects) are to be avoided in the design of elastically coupled rotor blades. The simplest laminate family which provides hygrothermal stability along with elastic couplings is the $[\theta, \theta + 90]$ family. To simplify the present study, the composite material is assumed to be woven cloth, rotated off-axis, so that $[\theta, \theta + 90]$ is contained in a single ply.

There are several types of laminate designs using the $[\theta, \theta + 90]$ family which are capable of producing elastic couplings, but the present study considers only symmetric and antisymmetric ply layup configurations composed of cloth material. These laminates are hygrothermally stable and the dominant coupling terms are contained in the *A-matrix* terms of classical laminate theory (ref. 10). These terms are referred to as extension stiffnesses in classical laminate theory, and the global elastic couplings of the blade are developed by lamina design in which local extension forces produce appropriate local shear strains.

To understand how elastic couplings are developed in rotor blades, it is convenient to examine the force-deformation relationships of composite laminates on both a local and a global level. A simple truss analogy is shown in figure 1 to help explain how bending-twist coupling is created by using off-axis composite plies. As shown, a rotor blade section is assumed to be composed of a composite laminate rotated off-axis in the same direction on both the upper and lower surfaces. At any section of the blade undergoing flap-down bending, the bending moment can be translated into a force-couple such that the upper surface has a tension force and the lower surface has a compressive force (global force is the sum of local forces). Looking only at the upper surface, the composite material may be modeled as a simple truss with two crossing rod members. One rod is extensionally stiff and represents the fiber direction, and the other rod is extensionally flexible and represents the matrix direction. A tensile force on this truss model can be seen not only to extend the truss but also to shear it in the direction of the flexible rod member. The shear strains are consistent along the entire upper surface of the airfoil, thus creating a shear flow which tends to twist the blade nose down. The lower surface is in compression rather than tension. The material fiber direction on this surface is the same as it is on the upper surface; therefore, in compression the shear flow is in the opposite direction from the upper surface and also produces nose-down twist. The bending-twist coupling illustrated in figure 1 is flapwise-bending-twist coupling such that bending up produces nose-up twist. Bending-up nose-down twist is created by reversing the fiber angles to the negative values of those illustrated in the figure.

The laminate construction described above is referred to as symmetric because the ply angles of the composite laminates contributing to elastic couplings in both the upper and lower surfaces of the model (above and below the flapwise neutral axis) are oriented in the same direction with respect to the principal blade axis. In antisymmetric laminate construction, the composite laminates in the lower and upper surfaces have ply angles of opposite signs. Such an antisymmetric configuration would produce extension-twist coupling rather than bending-twist coupling. Extension-twist coupling can be explained by using the same truss model shown in figure 1, except that the bending-moment couple is replaced by extension forces on both the upper and lower surfaces which lead to the same shear flow pattern illustrated on the bottom of the figure.

Note that parasitic or secondary couplings are generally associated with the primary structural coupling introduced with off-axis plies. Referring once again to figure 1, it can be seen that a symmetric configuration would produce not only flapwise-bending-twist coupling, but also extension-chordwise-shear coupling because the local shear of the laminates would flow in the same direction if extension force is produced on both upper and lower surfaces. An antisymmetric configuration would produce not only extension-twist coupling but also flapwise-bending-to-chordwise-shear coupling by similar reasoning. The extension-chordwise-shear and flapwise-bending-twist couplings are considered parasitic or secondary couplings because their magnitudes are small when compared to the primary elastic couplings. While these couplings to the global shear deformation are present, they may generally be ignored in rotor blade analytical modeling because bending and twist dominate the dynamics (as long as the cross-section analysis accounts for shear deformation effects in the calculation of the classical beam stiffnesses). The shear and extension modes are generally at such a high frequency that they have

a negligible influence on rotor blade performance, loads, and stability.

Another parasitic coupling associated with an antisymmetric laminate design is chordwise-bending-twist coupling. This coupling arises because of the unsymmetric distribution of the composite laminates with respect to the chordwise neutral axis position, caused by the airfoil shape of both the spar and skin, and also by the vertical web of the D-spar. Again, the chordwise-bending-twist coupling of an antisymmetric laminate design is referred to as parasitic because its magnitude is small compared to the primary coupling (extension twist). Elastic coupling, in which chordwise-bending twist is the primary coupling, can be created by using laminates which vary from symmetric to antisymmetric about the chordwise neutral axis position.

Approach of Present Study

Two baseline rotor blade designs which incorporate typical rotor blade cross sections were defined to serve as the basis for the present study. Key geometrical and laminate design variables of these baseline blades were systematically varied, and the resulting blade cross sections were analyzed. Trends in blade-elastic-coupling parameters and stiffnesses with respect to blade design variables were determined, and the results were summarized in graphs which should prove useful to both the designer and the researcher.

Blade cross sections were analyzed by using a finite-element analytical model which provides all classical beam stiffnesses and also the stiffnesses associated with elastic couplings (ref. 9). Because of the large number of blade design parameters to be varied, a preprocessor code was written to generate the geometric and laminate input required by the finite-element code.

Description of Baseline Blade Designs

Since the results of this study are meant to serve as a preliminary design database for future composite rotor blade designers and researchers, a wide range of rotor blade cross-section geometries and laminate layups have been considered. Baseline blade cross sections have been defined to provide a basis of comparison as the geometrical and laminate variables are varied. The influences of elastic coupling were studied for two baseline blade designs, designated 1 and 2, which have cross sections representative of typical rotor blade construction. The geometry is the same for both baseline designs (fig. 2), and both are NACA 0012 airfoils. The blade is assumed to be composed of three components: a spar, a skin covering, and a core fill. The spar is the primary load-carrying member, while the primary role of the skin is to maintain the proper aerodynamic shape of the blade. Elastic couplings are introduced in the blade via off-axis plies in the spar and/or skin laminates.

Baseline design 1 has the characteristics listed in table 1 and the laminate design shown in figure 2(b). This design is typical of composite rotor blade construction in which the spar is made of stiff, high-strength graphite/epoxy (Gr/E) woven cloth, and the skin is made of smooth, pliable S-fiberglass/epoxy (S-glass) woven cloth. The core material is honeycomb and is typical of that used in both full-scale and model-scale rotor blades. Table 2 lists the properties of the primary materials used in this study. A 14-in. chord was chosen because it is in a middle range between the largest full-scale designs and the smallest model-scale designs. The 35-percent spar width is typical of rotor blades because it provides an appropriate chordwise placement of the blade elastic axis. The spar thickness and the skin thickness generally are selected based on strength and frequency considerations, and those selected for baseline design 1 fall within ranges which are typical for composite blades. The laminate of the baseline design 1 blade is assumed to consist solely of 0° plies so that the influence of elastically coupled layups can be defined more clearly. In studies associated with baseline design 1, variations in ply angle orientation are for the entire thickness of the laminate, in both the spar and skin materials, unless otherwise stated.[1]

A more realistic composite blade is constructed of a combination of 0° and ±45° plies so that it has sufficient stiffness in both torsion and bending simultaneously. Furthermore, it is likely that any elastically coupled blade would not have all the plies in a laminate oriented at the same off-axis angle but would have only a certain percentage of plies devoted to inducing the desired level of elastic coupling. Baseline design 2 is defined to investigate elastic couplings and their influence on these more realistic assumptions, namely the inclusion of ±45° plies in combination with plies contributing to the elastic coupling and plies oriented at 0°. The characteristics of baseline design 2 are summarized in table 3 and the laminate design is shown in figure 2(c). They are very similar to the characteristics of baseline design 1 except that the skin laminate is composed of a 50-50 mix of 0° and ±45° plies (which do not change in the parametric study), and the spar parametric variables have been arranged to include ±45° plies in the spar.

[1]Woven cloth material is used throughout this study. Therefore, when a ply orientation angle θ is referred to, it implies a ply of woven cloth at $[\theta, \theta + 90]$.

As mentioned above, the parametric study associated with baseline design 1 centers on determining trends in coupling and stiffness in composite rotor blades as blade design variables are varied. Both symmetric and antisymmetric laminate construction are considered, and design variables are varied on baseline design 1 as follows: chord length c, spar width w_s, off-axis ply angle θ, ratio of spar and skin plies contributing to the elastic coupling $(\zeta_\theta)_{\mathrm{sp,sk}}$, and core material selection (51 foam core, 200 foam core, and balsa spar core). A balsa spar core (core inside of spar) is considered as a design variable in the present studies because balsa is often used as a core material in model-scale blades. For baseline design 2, both symmetric and antisymmetric layups are again considered, and design variables are varied as follows: off-axis ply angle θ in combination with the ratio of 0° plies in the spar $(\zeta_0)_{\mathrm{sp}}$, the ratio of $\pm 45^\circ$ plies in the spar $(\zeta_{45})_{\mathrm{sp}}$, and the ratio of plies contributing to coupling in the spar $(\zeta_\theta)_{\mathrm{sp}}$.

Description of Analysis

The results presented in this study were obtained by using a composite blade cross-section analysis based on the analytical model presented in reference 9. This model is ideally suited for the analysis of rotor blades in which the cross section is generally composed of an irregular outer contour and a complex internal structure. As discussed in reference 9, displacement solutions are written in terms of so-called *derivable functions* that represent extension, bending, twisting, and general functions for the in-plane and out-of-plane warping. The derivable functions depend on the shape of the cross-section planform, Poisson's ratio, pretwist angle, and pretwist axis location and are determined by solving a coupled two-dimensional boundary-value problem. Twist rate effects are generally small and were not considered in the present study. Ritz method solutions of the boundary-value problem are calculated by applying the principle of minimum potential energy to a discretized representation of the cross section. The elastic coupled stiffnesses are then determined by solving the equations of equilibrium for the blade cross section about the blade centroidal axes.

For the present study, only the coupled stiffness matrix calculated by the cross-section analysis is required. This matrix satisfies the relation

$$\begin{bmatrix} k_{11} & k_{12} & k_{13} & k_{14} \\ k_{21} & k_{22} & k_{23} & k_{24} \\ k_{31} & k_{32} & k_{33} & k_{34} \\ k_{41} & k_{42} & k_{43} & k_{44} \end{bmatrix} \begin{Bmatrix} e \\ \kappa_\zeta \\ \kappa_\eta \\ \theta \end{Bmatrix} = \begin{Bmatrix} P \\ M_\eta \\ M_\zeta \\ M_z \end{Bmatrix} \qquad (1)$$

where [**k**] is the coupled stiffness matrix and is always symmetric. In this equation, e is extension, κ_ζ and κ_η are bending curvatures, θ is the twist rate, P is tensile force, M_η and M_ζ are bending moments, and M_z is torsional moment. For an isotropic, untwisted beam the elastic twist is independent of the extension and bending ($k_{14} = k_{24} = k_{34} = 0$), and the diagonal terms represent the classical extension stiffness ($k_{11} = EA$), bending stiffnesses ($k_{22} = EI_f$, $k_{33} = EI_c$), and torsion stiffness ($k_{44} = GJ$). The remaining off-diagonal terms couple extension to bending ($k_{13} = EA_\zeta$, $k_{12} = -EA_\eta$) and bending in one plane to bending in the other ($k_{23} = -EI_{\zeta\eta}$). These last three terms are used in the analysis to calculate the centroid and principal axes of the cross section.

To facilitate the analysis of the various rotor blade cross sections which were to be considered in the parametric study, a subroutine was written to generate the geometry of a two-dimensional finite-element model of a blade cross section. This geometry code is called from within a main program to directly provide the finite-element analysis subroutine with the necessary nodes, elements, ply material, and ply orientation angles to adequately discretize a rotor blade cross section. This code represents a great improvement over the rather tedious method of developing an input file for the finite-element code and allows for easy analysis of almost any composite rotor blade cross section with or without a D-spar. The complete code allows the consecutive analysis of many cross sections in which the principal design variables mentioned above are varied. In this manner, the sensitivity of the classical stiffnesses and couplings of composite rotor blades to these principal variables is determined. The principal variables that the code requires are as follows: chord length, airfoil thickness, number of chordwise divisions, width of spar, number of plies in skin and spar, thickness of skin and spar plies, skin and spar ply materials, skin and spar ply orientation angles (upper and lower), spar core material, and aft core material.

Nondimensional Parameters

For the results of this study to be applicable to any size rotor blade cross section, the computed results for both classical stiffnesses and coupling stiffnesses are presented in nondimensional form. Following reference 11, nondimensional coupling parameters can be defined for each type coupling by considering the appropriate two degree-of-freedom subsets of equations from equation (1). For example,

for the case of extension-twist coupling, the appropriate equations would be

$$\begin{Bmatrix} P \\ M_z \end{Bmatrix} = \begin{bmatrix} EA & k_{14} \\ k_{14} & GJ \end{bmatrix} \begin{Bmatrix} e \\ \theta \end{Bmatrix} \tag{2}$$

Equation (2) relates the axial force and twisting moment to the extension and twist rate of the cross section. This equation can be inverted to obtain the flexibility relation

$$\begin{Bmatrix} e \\ \theta \end{Bmatrix} = \frac{1}{1-ab} \begin{bmatrix} \frac{1}{EA} & \frac{-b}{EA} \\ \frac{-b}{EA} & \frac{1}{GJ} \end{bmatrix} \begin{Bmatrix} P \\ M_z \end{Bmatrix} \tag{3}$$

where $a = \frac{k_{14}}{EA}$ and $b = \frac{k_{14}}{GJ}$. The term $(1 - ab)$ must be greater than zero to satisfy strain-energy considerations. The product ab can be expressed as an extension-twist coupling parameter Ψ_{ET} which is defined as follows:

$$\Psi_{ET}^2 = \frac{k_{14}^2}{EAGJ} < 1 \tag{4}$$

By writing equations similar to equation (2) for coupled flapwise-bending-twist and chordwise-bending-twist and by proceeding as shown above, nondimensional coupling parameters Ψ_{FT} and Ψ_{CT} can be defined as

$$\Psi_{FT}^2 = \frac{k_{24}^2}{EI_f GJ} < 1 \tag{5}$$

$$\Psi_{CT}^2 = \frac{k_{34}^2}{EI_c GJ} < 1 \tag{6}$$

Because of the requirement that strain energy be positive, it can be seen that all three nondimensional parameters Ψ_{ET}, Ψ_{FT}, and Ψ_{CT} are bounded such that

$$-1 < \Psi < 1 \tag{7}$$

The three coupling parameters defined in equations (4) through (6) are used to define the magnitude, type, and direction of coupling in a given configuration. By knowing the baseline stiffnesses of a blade, one can easily determine the coupling stiffnesses by knowing the nondimensional coupling parameters. Therefore, the results of the present study can be used to determine the magnitude of coupling in a rotor blade for a given value of the nondimensional coupling parameter.

An important aspect of the laminate design is the influence of elastic couplings on the classical stiffness terms EI_f, EI_c, and GJ. The classical stiffnesses significantly influence rotor blade dynamics, and as a result there is generally a narrow range of acceptable stiffness values and distributions for a particular design. It is therefore important to understand and to determine the effect of structural coupling on the baseline blade stiffnesses. As an example, for an uncoupled rotor blade the flapwise bending stiffness EI_f is the ratio of the bending moment M_η to the spanwise curvatures κ_ζ. With flapwise-bending-twist coupling introduced, the effective bending stiffness may be defined by the same ratio, but in terms of the uncoupled bending stiffness the ratio becomes

$$\frac{M_\eta}{\kappa_\zeta} = EI_f \left(1 - \Psi_{FT}^2\right) \tag{8}$$

The coupling is seen to reduce the effective bending stiffness and will also reduce the associated bending frequency of a rotor blade. Similar effects occur for the chordwise bending stiffness and the extensional stiffness when those degrees of freedom are coupled with twist.

The present study examines the influence of elastic coupling on uncoupled blade stiffnesses. Insight into this influence is aided by introducing the three nondimensional stiffness ratios

$$\frac{EI_f}{(EI_f)_o}, \frac{EI_c}{(EI_c)_o}, \text{ and } \frac{GJ}{(GJ)_o}$$

where the subscript o refers to the uncoupled baseline stiffnesses defined for the study. Together with the elastic coupling parameters, these stiffness ratios can be applied to many rotor blade designs.

Results of Parametric Study

The results of the parametric studies are presented in this section. First, the trends in elastic couplings and stiffnessess for the baseline design 1 blade are presented and discussed. Both symmetric and antisymmetric laminate construction are considered for this blade design. Next, the trends in elastic couplings and stiffnesses of the baseline design 2 blade are discussed. Again, both symmetric and antisymmetric laminate construction are considered.

The effect of the number of chordwise divisions δ in the finite-element model of the cross section on the stiffnesses and coupling parameters was investigated first to identify the minimum number of chordwise divisions which could be used to model the blade accurately. Figure 3 illustrates the variation of Ψ_{FT} as a function of the ply orientation angle as the number of chordwise divisions is increased in a model

of the skin only. It can be seen that at $\delta = 16$ the coupling parameter has converged to its final value. Referring to figures 4 and 5, the flapwise flexural stiffness can be seen to converge at $\delta = 24$ and the torsional stiffness can be seen to converge at approximately $\delta = 24$. Based on these results, it was decided to use 24 chordwise divisions in the finite-element model.

Symmetric Cases for Baseline Design 1

For this part of the study, the baseline design 1 cross section with symmetric laminate construction is analyzed. Table 4 lists all stiffness values for the baseline design 1 rotor blade cross section. Cross sections with symmetric laminate construction have a flapwise-bending-twist coupling whose magnitude depends on the value and sign of the ply orientation angle. Figures 6 and 7 illustrate the trends in EI_f, EI_c, GJ, and k_{24} as the ply orientation angle is varied in the baseline 1 cross section. Unless otherwise stated, it is assumed that all the plies in the spar and the skin contribute to the coupling.

Trends caused by chord variation. Figure 8 illustrates the trend in Ψ_{FT} as a function of the ply orientation angle for blade chord lengths of 4, 14, and 20 in.; Ψ_{FT} was found to be independent of the length of the blade chord as long as t_{sk} and t_{sp} remain constant (if the laminate thicknesses are scaled as the chord is increased). The independence of Ψ_{FT} with blade chord may be explained with the aid of figures 9 through 11. These figures show that the flapwise flexural, chordwise flexural, and torsional stiffness ratios remain constant as the ply orientation angle is increased, and consequently as Ψ_{FT} is increased, although the dimensional stiffness values increase because of the greater chord. Since all stiffness ratios increase proportionately as the chord and ply orientation angle are increased, Ψ_{FT} remains constant with chord length for composite blades.

Relative contributions of spar and skin to coupling. Figure 12 illustrates the amount of coupling that is contributed by the skin and spar separately, as compared to the baseline cross section in which all the plies contribute to the elastic coupling. The greatest amount of coupling Ψ_{FT} is contributed by the spar since the composite material in the spar is graphite/epoxy cloth, which is much stiffer than the S-glass cloth composite in the skin. The baseline blade can be seen to be a compromise between the graphite spar and the less stiff S-glass skin.

Trends caused by spar width variation. Since the width of D-spars in modern rotor blades varies considerably from one blade design to another, the effects of spar width on both Ψ_{FT} and blade stiffness is of interest. Figure 13 illustrates the variation of Ψ_{FT} with ply orientation angle as the width of the spar is varied. As can be seen, the increased spar width results in an increase in the coupling for the baseline blade. This result indicates that increasing the spar width increases the blade flapwise-bending-twist-coupled stiffness by an amount which is greater than the product of the bending and torsion stiffnesses.

Trends in the stiffness ratios are illustrated in figures 14 through 16. For a given amount of coupling Ψ_{FT}, it is seen that a greater flexural stiffness ratio can be achieved by using small ply orientation angles. However, the magnitude of the torsional stiffness ratio is less for the same amount of coupling Ψ_{FT}. Consequently, for a given stiffness ratio, a larger coupling can be achieved with an increased spar width. These results suggest that increasing the spar width is a means of increasing the coupling within stiffness limitations for composite rotor blades.

Trends caused by laminate variation. As expected, the ply orientation angle has a significant impact on the degree of elastic coupling within a composite rotor blade. Referring to figure 8, it can be seen that the coupling is zero at ply orientation angles of 0° and 45° and the value of coupling is maximum at approximately 22.5° (for any chord length). This trend is as expected because at ply angles of 0° the fibers embedded in the composite material are aligned with the loading and thus do not shear under applied compressive or tensile load. At a ply angle of 45°, the fibers are also aligned with the loading such that they do not shear. While the maximum coupling occurs with ply orientation angles around 22.5°, it is generally not feasible to use such ply angles because of decreased bending stiffness. Figures 9 through 11 illustrate that the blade's flapwise and chordwise flexural stiffnesses decrease by approximately 30 and 50 percent and that the torsional stiffness increases by approximately 250 percent compared with the baseline values.

The practical limit for Ψ_{FT} can also be determined by referring to figures 9 through 11, which illustrate the change in stiffness ratios as ply orientation angle is varied. These plots show that the flexural stiffness ratios do not vary greatly from 1.0 for values of Ψ_{FT} up to about 0.2. For design purposes, an allowable change in bending stiffness is usually known, and the corresponding maximum value of the coupling parameter can then be deduced from these plots. In general, the results for composite blades with symmetric layups suggest that the theoretical

limit of Ψ_{FT} is 0.55 and that the practical limit when blade stiffness is considered is approximately 0.2.

Another variable which is of importance in the design of elastically coupled composite rotor blades is the fraction of plies in the layup which contribute to the coupling. This variable can be expressed as the ratio of plies ζ_θ that are oriented at an angle off-axis from the principal axis. For the purposes of this part of the study, plies in both the skin and the spar may contribute to the coupling; therefore, $(\zeta_\theta)_{\mathrm{sp,sk}}$ is varied. Figure 17 illustrates the trends in Ψ_{FT} versus ply orientation angle as $(\zeta_\theta)_{\mathrm{sp,sk}}$ is increased from 0.2 to 1.0 for the baseline blade. The maximum value of the coupling (at $\theta = 22.5°$) is seen to increase relatively linearly as the percentage of plies contributing to the coupling is increased. The trends in stiffness ratios versus Ψ_{FT} as $(\zeta_\theta)_{\mathrm{sp,sk}}$ is increased are shown in figures 18 through 20. As the percentage of plies contributing to the coupling is increased, the flexural stiffness ratios at maximum Ψ_{FT} decrease considerably while the torsional stiffness ratio increases. From these results it can be concluded that it is best to have all the plies contribute to the coupling since this condition results in the least loss of flexural stiffness and the least increase in torsional stiffness for the desired degree of coupling.

Trends caused by variation of core material. Since different blade designs tend to have different core materials, depending on whether the blade is a model, a full-scale tilt-rotor, or a full-scale helicopter blade, it is important to study the effects of core material on coupling and stiffness. Figure 21 illustrates the effect of using three different core materials, as compared to the baseline blade, which has a honeycomb aft core and a hollow spar. A blade with both 51 and 200 Rohocell foam aft cores and a blade with a honeycomb aft core and balsa spar core (to represent a model blade) were considered. As can be seen, there is little effect on Ψ_{FT} as the core materials are varied, and there was little change in the stiffness ratios. Therefore, the core material has little effect on the flapwise-bending-twist coupling parameter Ψ_{FT}.

Antisymmetric Cases for Baseline Design 1

For this part of the study, the baseline blade listed in table 1 was generated by using the cross-section geometry code with antisymmetric laminate construction. The stiffness properties of this baseline blade are the same as those listed in table 4 because for a zero-ply orientation angle, the blade is identical to the one analyzed in the symmetric part of the study. Figures 22 and 23 illustrate the trends in stiffness as the ply orientation angle of the baseline blade is varied from 0° to 45°. As expected, the antisymmetric blade resulted in an extension-twist coupling whose magnitude depends on whether the ply orientation angle is positive or negative. A secondary coupling, Ψ_{CT} or chordwise-bending-twist coupling, was also found. The physical interpretation of this coupling is discussed later in this section.

Trends caused by chord variation. Figures 24 and 25 illustrate Ψ_{ET} and Ψ_{CT} versus ply orientation angle and figures 26 through 28 illustrate the stiffness ratios versus ply orientation angle as the length of the blade chord is varied. Like the coupling in symmetric laminate blades, Ψ_{ET} and Ψ_{CT} do not vary with chord. The physical interpretation of this phenomenon is the same as in the symmetric case. Since all coupling parameters are independent of chord, the results of this study can be applied to rotor blades of any chord length.

Trends caused by variation of spar width. The effect of increasing the spar width on Ψ_{ET} is illustrated in figure 29. The extension-twist coupling parameter is seen to increase nonlinearly as the spar width is increased. As in the symmetric laminate case, the increased spar width results in an increase in the coupling and consequently in an increase in Ψ_{ET} for the baseline blade. This result indicates that increasing the spar width increases the blade extension-twist coupled stiffness by an amount which is greater than the product of the extension and torsion stiffnesses. Thus, increasing the spar width is a viable means for increasing the extension-twist coupling of a composite blade.

The nondimensional chordwise-bending-twist coupling parameter Ψ_{CT} was found to be more affected by a change in the spar width. Referring to figure 30, Ψ_{CT} is shown to increase as the spar width ratio is increased from 0.20 to 0.35 and to decrease as the spar width ratio is increased from 0.35 to 0.50. Therefore, Ψ_{CT} is maximized somewhere between a spar width ratio of 0.35 and 0.50. This behavior in the chordwise-bending-twist coupling is associated with the shift in the chordwise position of the neutral axis. The neutral axis is shifted aft as the spar width is increased, thereby also increasing the amount of the cross section that is in tension while decreasing the amount in compression. Furthermore, as the spar width is increased, more of the spar extends aft of the neutral axis, and the resulting increase in the amount of composite material in compression adds to the chordwise-bending-twist coupling. The shift in the neutral axis position and in the aft location of the spar is listed in table 5. The presence of this

secondary coupling, chordwise-bending-twist, in antisymmetric composite rotor blades is a characteristic that has not been discussed greatly in past research.

Referring to figures 31 and 32, trends in both Ψ_{ET} and Ψ_{CT} versus ply orientation angle are shown for the baseline blade, the spar only, and the skin only; Ψ_{ET} behaves as expected, with the relatively soft skin contributing less coupling to the baseline blade than the graphite spar contributes. However, Ψ_{CT} is to be almost zero for the skin and spar-only cases. This trend supports what has been concluded above, namely, that the chordwise position of the neutral axis has a strong influence on the chordwise-bending-twist coupling parameter. For the skin-only case, the neutral axis is near the mid chord. Equal areas of the skin are then in compression and tension under a chordwise bending load, and the shear flow that arises from this loading is nearly zero. Therefore, the chordwise-bending-twist coupling parameter is zero for the skin-only case, and by similar reasoning, this is also true for the spar-only case. However, when both the skin and the spar are present, as in the baseline blade, the location of the neutral axis is shifted to a position which gives unequal areas under compression and tension for chordwise bending, and thus chordwise-bending-twist coupling is present.

The effects of increasing the spar width on blade stiffness ratios are shown in figures 33 through 35. Increasing the spar width and therefore the coupling parameters results in a slight decrease in both flapwise and chordwise flexural stiffness ratios; the decrease becomes more evident as the ply orientation angle is increased. The torsional stiffness ratio increases slightly as the spar width is increased, with the increase becoming more evident as the ply orientation angle is increased.

It has been shown that increasing the width of the spar is a means of increasing both the extension-twist and chordwise-bending-twist coupling parameters while also increasing the blade stiffness. Stiffness ratios were found not to vary far from baseline values for values of $\Psi_{ET} \leq$ about 0.2. It can be concluded that increasing the spar width is a viable way to increase antisymmetric coupling parameters while maintaining reasonable values of stiffness ratio.

Trends caused by laminate variation. As in the symmetric case of Ψ_{FT}, the antisymmetric coupling parameters are zero at ply orientation angles of 0° and 45°. Referring to figures 24 and 25, Ψ_{ET} was found to be maximum (0.55) at about $\theta = 22.5°$, and Ψ_{CT} was found to be maximum (0.16) at approximately $\theta = 25.0°$. Figures 26 through 28 show that at the maximum values of the coupling parameters the blade stiffness ratios are greatly reduced, which may be unacceptable from a blade dynamics standpoint. Therefore, the physical limits of Ψ_{ET} and Ψ_{CT} may not be practical because of stiffness limitations. A more practical limit of the coupling parameters can be determined by referring again to the stiffness ratios. Keeping in mind that the stiffnesses generally cannot vary greatly from the baseline values, the practical limit of Ψ_{ET} is approximately 0.2 and the practical limit of Ψ_{CT} is approximately 0.1.

Figure 36 illustrates Ψ_{ET} versus ply orientation angle as the percentage of plies in the skin and spar contributing to the coupling $(\zeta_\theta)_{\mathrm{sp,sk}}$ is increased from 0.2 to 1.0. The maximum value of the extension-twist coupling parameter (at $\theta = 22.5°$) is seen to increase fairly linearly as $(\zeta_\theta)_{\mathrm{sp,sk}}$ is increased. In figure 37, Ψ_{CT} is seen to increase nonlinearly as $(\zeta_\theta)_{\mathrm{sp,sk}}$ is increased. Figures 38 through 40 illustrate the trends in stiffness ratios versus Ψ_{ET} as $(\zeta_\theta)_{\mathrm{sp,sk}}$ is increased. As the percentage of plies contributing to the coupling is increased, the flexural stiffness ratios at maximum Ψ_{ET} decrease considerably while the torsional stiffness ratio increases considerably. From these stiffness and coupling results, it can be concluded that it is best to have all the plies contribute to the coupling. Having all the plies contribute to the coupling results in the least loss of flexural stiffness and in the least increase in torsional stiffness, which is important to the aeroelastic stability of rotor blade systems.

Trends caused by variation of core material. Figures 41 and 42 illustrate the sensitivity of Ψ_{ET} and Ψ_{CT} to the core material. Again, the core materials investigated are the baseline honeycomb, the 51 Rohocell foam, the 200 Rohocell foam, and the balsa spar core. The extension-twist coupling parameter does not vary dramatically as the type of core is changed in the baseline blade. On the other hand, Ψ_{CT} is very dependent on the type of core material. This dependence results from the sensitivity of Ψ_{CT} to the position of the neutral axis, as discussed earlier. Since the density and the stiffness of the different core materials tend to shift the neutral axis fore and aft of the baseline position, the chordwise coupling is therefore dependent on the type of core material.

Symmetric and Antisymmetric Cases for Baseline Design 2

The laminate variables $(\zeta_\theta)_{\mathrm{sp,sk}}$ have been shown to have a great effect on both the coupling and the stiffness of a blade and to offer a practical method for elastically tailoring composite rotor blades. However, there are other laminate properties which can be

varied to affect coupling and stiffness, and these are also of interest to blade designers. Current composite blade designs generally have plies that are oriented at angles of $\pm 45^\circ$ and future elastically coupled blades also will likely have plies at other off-axis angles that contribute to the coupling. These laminate variations are the subject of this part of the study, specifically: $(\zeta_\theta)_{\rm sp}$, $(\zeta_{45})_{\rm sk}$, $(\zeta_0)_{\rm sk}$, $(\zeta_{45})_{\rm sp}$, and $(\zeta_0)_{\rm sp}$. As discussed previously, a second baseline blade was defined whose characteristics can be found in table 3. This blade has constant skin laminate characteristics and variable spar laminate characteristics. Table 6 lists the stiffness properties for the baseline design 2 blade. Trends in these stiffness properties (as several laminate variables are varied) will be investigated for both symmetric laminates (flapwise bending-twist coupled) and antisymmetric laminates (extension-twist and chordwise bending-twist coupled).

Trends caused by variation of $(\zeta_\theta)_{\rm sp}$ on baseline design 2 blade. Trends in Ψ_{FT} as $(\zeta_\theta)_{\rm sp}$ is increased from 0.2 to 1.0 are illustrated in figure 43 for a composite rotor blade with symmetric laminate construction. The maximum value of Ψ_{FT} (at $\theta = 22.5^\circ$) is found to increase fairly linearly as $(\zeta_\theta)_{\rm sp}$ is increased, and as expected, the minimum values of Ψ_{FT} were found at $\theta = 0^\circ$ and $\theta = 45^\circ$. Figures 44 through 46 illustrate the trends in stiffness ratios versus Ψ_{FT} as $(\zeta_\theta)_{\rm sp}$ is increased. The least loss in flexural stiffness and the least increase in torsional stiffness occur when $(\zeta_\theta)_{\rm sp} = 1.0$, as concluded in previous sections, but this value of $(\zeta_\theta)_{\rm sp}$ may not always be desirable in the complete blade design.

Figures 47 and 48 illustrate the trends in Ψ_{ET} and Ψ_{CT} as $(\zeta_\theta)_{\rm sp}$ is varied from 0.2 to 1.0 for an antisymmetric layup. Again, the maximum value of Ψ_{ET} was found to increase fairly linearly with $(\zeta_\theta)_{\rm sp}$ while the maximum value of Ψ_{CT} was found to increase nonlinearly for the baseline blade. Figures 49 through 51 show the trends in stiffness ratios versus Ψ_{ET} as $(\zeta_\theta)_{\rm sp}$ is increased. Again, as above, the least loss in flexural stiffness and the least increase in torsional stiffness occur when $(\zeta_\theta)_{\rm sp} = 1.0$, but other blade designs may be more desirable. The presence of plies within the laminate at orientation angles of $\pm 45^\circ$ must also be investigated.

Trends caused by variation of $(\zeta_\theta)_{\rm sp}$ and $(\zeta_{45})_{\rm sp}$ on baseline design 2 blade. Since $\pm 45^\circ$ oriented plies can be found in all composite rotor blades, the effect on coupling and stiffness of various amounts of these plies, along with plies which contribute to the coupling, must be investigated. In this section, the laminate variables $(\zeta_\theta)_{\rm sp}$ and $(\zeta_{45})_{\rm sp}$ within the spar of the baseline 2 blade will be varied from 0.0 to 1.0. The effects on the trends in coupling parameters and stiffness ratios will be presented in plots of lines of constant Ψ_{FT} or Ψ_{ET} and stiffness ratios versus $(\zeta_\theta)_{\rm sp}$ and $(\zeta_{45})_{\rm sp}$.

Figure 52 illustrates lines of constant Ψ_{FT} versus $(\zeta_\theta)_{\rm sp}$ and $(\zeta_{45})_{\rm sp}$ for a blade with a symmetric layup. As expected, increasing $(\zeta_\theta)_{\rm sp}$ increases the flapwise-bending-twist coupling parameter. Increasing $(\zeta_{45})_{\rm sp}$ had little effect on Ψ_{FT} for small degrees of coupling but had an increasing effect as Ψ_{FT} was increased. This increasing sensitivity of Ψ_{FT} to $(\zeta_{45})_{\rm sp}$ is evident in the increasingly bowed lines of constant Ψ_{FT} as coupling is increased. For antisymmetric layups, figures 53 and 54 illustrate lines of constant Ψ_{ET} and Ψ_{CT} versus $(\zeta_\theta)_{\rm sp}$ and $(\zeta_{45})_{\rm sp}$. Again, the increasing sensitivity of the coupling parameters to $(\zeta_{45})_{\rm sp}$ is indicated by the increasingly bowed lines.

Lines of constant stiffness ratios versus $(\zeta_\theta)_{\rm sp}$ and $(\zeta_{45})_{\rm sp}$ for the symmetric layup are illustrated in figures 55 through 57. Lines of constant Ψ_{FT} are also shown in order to illustrate the global effect on both the coupling parameters and the stiffness ratios of varying values of $(\zeta_\theta)_{\rm sp}$ and $(\zeta_{45})_{\rm sp}$. Both the decrease in the flexural stiffness ratio and the increase in the torsional stiffness ratio resulting from an increase in either (or both) $(\zeta_\theta)_{\rm sp}$ and $(\zeta_{45})_{\rm sp}$ are evident.

Figures 58 through 60 illustrate lines of constant stiffness ratios versus $(\zeta_\theta)_{\rm sp}$ and $(\zeta_{45})_{\rm sp}$ for antisymmetric layups. Lines of constant Ψ_{ET} are included to illustrate the global effect on coupling parameters and stiffness ratios of $(\zeta_\theta)_{\rm sp}$ and $(\zeta_{45})_{\rm sp}$. Both the decrease in the flexural stiffness and the increase in the torsional stiffness resulting from an increase in either (or both) $(\zeta_\theta)_{\rm sp}$ and $(\zeta_{45})_{\rm sp}$ are evident.

As discussed above, figures 55 through 60 illustrate both lines of constant stiffness ratio and coupling parameter versus $(\zeta_\theta)_{\rm sp}$ and $(\zeta_{45})_{\rm sp}$. These plots provide a great deal of information concerning trends in coupling and stiffness when $(\zeta_\theta)_{\rm sp}$ and $(\zeta_{45})_{\rm sp}$ are varied and are applicable to any elastically coupled blades of similar construction. For lines of constant Ψ_{FT} and Ψ_{ET}, there exist many values of a stiffness ratio at a different value of both $(\zeta_\theta)_{\rm sp}$ and $(\zeta_{45})_{\rm sp}$. By varying $(\zeta_\theta)_{\rm sp}$ and $(\zeta_{45})_{\rm sp}$, it can be seen that an elastically coupled rotor blade can be tailored by using these figures to achieve a desired degree of coupling and stiffness in a design.

Conclusions

In this study, the effects of composite rotor blade laminate design parameters on elastic coupling and

classical beam stiffness have been determined by using a two-dimensional finite-element code. Results of the present study provide a preliminary design database so that the influences of elastic couplings based on representative composite blade designs can be studied easily. These results offer investigators a reasonably accurate knowledge of the potential for incorporating elastic couplings in existing blade designs without the need to design blade cross sections and perform cross-section analysis to obtain the required section properties.

Based on the results of this study, the following conclusions are drawn:

1. The theoretical limits for the nondimensional elastic coupling stiffnesses associated with representative rotor blade cross sections are about 0.6 for flapwise-bending-twist coupling and extension-twist coupling, and about 0.15 for chordwise-bending-twist coupling. With the importance of flexural and torsional stiffness considered, the practical limitations for the nondimensional elastic coupling stiffnesses associated with representative rotor blade cross sections are about 0.2 for flapwise-bending-twist coupling and extension-twist coupling, and about 0.1 for chordwise-bending-twist coupling.

2. Increasing ply orientation angle increases all coupling parameters, and the maximum coupling can be achieved at an angle of about 22.5°. As shown in past studies, the magnitude of the coupling is zero at angles of 0° and 45°, flexural stiffness is maximum at 0° and minimum at 45°, and torsional stiffness is minimum at 0° and maximum at 45°.

3. Variation of the airfoil chord length has no effect on the nondimensional coupling parameters for both symmetric and antisymmetric layups if the ratio of the skin and spar thickness to the length of the chord is held constant. These results suggest that the nondimensional coupling parameters introduced in this study can be applied to any size rotor blades.

4. Increasing spar width increases both the coupling stiffnesses and the bending stiffnesses. This effect may be used in combination with an increase in the ply orientation angles (which decrease bending stiffness) to increase the magnitude of coupling without adversely decreasing the bending stiffness.

5. The location of the neutral axis has a significant effect on the chordwise-bending-twist coupling.

6. Increasing the fraction of off-axis plies contributing to the coupling increases significantly the nondimensional coupled stiffness parameters and increases flexural stiffness for a desired level of elastic coupling.

7. The type of core material has only a small effect on the nondimensional coupled stiffness parameters.

8. Increasing the fraction of ±45° plies in the laminate has little effect on the nondimensional coupled stiffness parameters even though it has a significant effect on the actual coupled stiffnesses, flexural stiffnesses, and torsional stiffnesses themselves.

NASA Langley Research Center
Hampton, VA 23681-0001
December 16, 1996

References

1. Hong, C. H.; and Chopra, I.: Aeroelastic Stability Analysis of a Composite Rotor Blade. *J. Am. Helicopter Soc.*, vol. 30, Apr. 1985, pp. 57–67.

2. Hong, Chang-Ho; and Chopra, Inderjit: Aeroelastic Stability of a Composite Bearingless Rotor Blade. *J. Am. Helicopter Soc.*, vol. 31, Oct. 1986, pp. 29–35.

3. Hong, Chang-Ho: Aeroelastic Stability of Composite Rotor Blades. Ph.D. Diss., Univ. Maryland, 1985.

4. Panda, Brahmananda; and Chopra, Inderjit: Dynamics of Composite Rotor Blades in Forward Flight. *Vertica*, vol. 11, no. 1/2, 1987, pp. 187–209.

5. Ormiston, R. A.: Rotor-Fuselage Dynamic Coupling Characteristics of Helicopter Air and Ground Resonance. *Proceedings of the Theoretical Basis of Helicopter Technology*, AHS, Nov. 1985.

6 Ormiston, Robert A.: Aeromechanical Stability of Soft Inplane Hingeless Rotor Helicopters. *Third European Rotorcraft and Powered Lift Aircraft Forum*, Paper No. 25, Sept. 1977.

7. Smith, Edward C.: Aeroelastic Response and Aeromechanical Stability of Helicopters With Elastically Coupled Composite Rotor Blades. Ph.D. Diss., Univ. Maryland, 1992.

8. Nixon, Mark W.: Aeroelastic Response and Stability of Tiltrotors With Elastically-Coupled Composite Rotor Blades. Ph.D. Diss., Univ. Maryland, 1993.

9. Kosmatka, J. B.: On the Behavior of Pretwisted Beams With Irregular Cross-Sections. *J. Appl. Mech.*, vol. 114, Mar. 1992, pp. 146–152.

10. Jones, Robert M.: *Mechanics of Composite Materials*. Scripta Book Co., 1975.

11. Weisshaar, Terrence A.: Creative Uses of Unusual Materials. AIAA-87-0976, Apr. 1987.

Table 1. Characteristics of Baseline Design 1

Characteristic	Baseline value
c, chord length, in.	[a]14
w_s, spar width ratio	[a]0.35
Spar material	Graphite
Skin material	S-Glass
Core material	[a]Honeycomb
t_{sp}, spar thickness	0.00800
t_{sk}, skin thickness	0.00214
θ, laminate off-axis angle, deg	[a]0
$(\zeta_\theta)_{sp,sk}$ (ratio of coupling plies)	[a]0.0
$(\zeta_0)_{sp,sk}$ (ratio of 0° plies)	[a]1.0

[a]Indicates that parameter varied in study.

Table 2. Material Properties of Baseline Blades

Material property	Gr/E woven cloth	S-Glass/E woven cloth	Nomex honeycomb
Young's modulus (E11)	1.1640E+07 Msi	4.4500E+06 Msi	2.8000E+04 Msi
Young's modulus (E22)	1.1640E+07 Msi	4.3200E+06 Msi	2.8000E+04 Msi
Young's modulus (E33)	1.6255E+06 Msi	1.1000E+06 Msi	2.8000E+04 Msi
Shear modulus (G12)	9.0900E+05 Msi	6.9000E+05 Msi	4.7000E+04 Msi
Shear modulus (G13)	9.0900E+05 Msi	6.9000E+05 Msi	4.7000E+04 Msi
Shear modulus (G23)	9.0900E+05 Msi	6.9000E+05 Msi	4.7000E+04 Msi
Poisson ratio (v12)	4.6600E-02	1.1400E-01	3.0000E-01
Poisson ratio (v13)	3.2000E-01	2.7000E-01	3.0000E-01
Poisson ratio (v23)	3.2000E-01	2.7000E-01	3.0000E-01
Density, ρ	5.7810E-02 lb/in^3	6.5030E-02 lb/in^3	2.3150E-03 lb/in^3

Table 3. Characteristics of Baseline Design 2

Characteristic	Baseline value
c, chord length, in.	14
w_s, spar width ratio	0.35
Spar material	Graphite
Skin material	S-Glass
Core material	Honeycomb
t_{sp}, spar thickness	0.00800
t_{sk}, skin thickness	0.00214
θ, laminate off-axis angle, deg	[a]0
$(\zeta_\theta)_{sp}$ (ratio of spar coupling plies)	[a]0.0
$(\zeta_{45})_{sk}$ (ratio of ±45° skin plies)	0.5
$(\zeta_0)_{sk}$ (ratio of 0° skin plies)	0.5
$(\zeta_{45})_{sp}$ (ratio of ±45° spar plies)	[a]0.0
$(\zeta_0)_{sp}$ (ratio of 0° spar plies)	[a]1.0

[a]Indicates that parameter varied in study.

Table 4. Baseline Design 1 Stiffness Properties
About the Blade Centroidal Axes

Stiffness	Value
EI_F, lb-in^2	7.11E + 06
EI_c, lb-in^2	1.47E + 08
GJ, lb-in^2	2.40E + 06
k_{14}, lb-in.	0.0E + 00
k_{24}, lb-in^2	0.0E + 00
k_{34}, lb-in^2	0.0E + 00

Table 5. Shift of Neutral Axis and Spar

w_s, percent	Neutral axis position (x/c)	Spar position (x/c)
20	0.264	0.200
35	.286	.350
50	.314	.500

Table 6. Baseline Design 2 Stiffness Properties
About the Blade Centroidal Axes

Stiffness	Value
EI_F, lb-in^2	6.84E + 06
EI_c, lb-in^2	1.26E + 08
GJ, lb-in^2	3.16E + 06
k_{14}, lb-in.	0.0E + 00
k_{24}, lb-in^2	0.0E + 00
k_{34}, lb-in^2	0.0E + 00

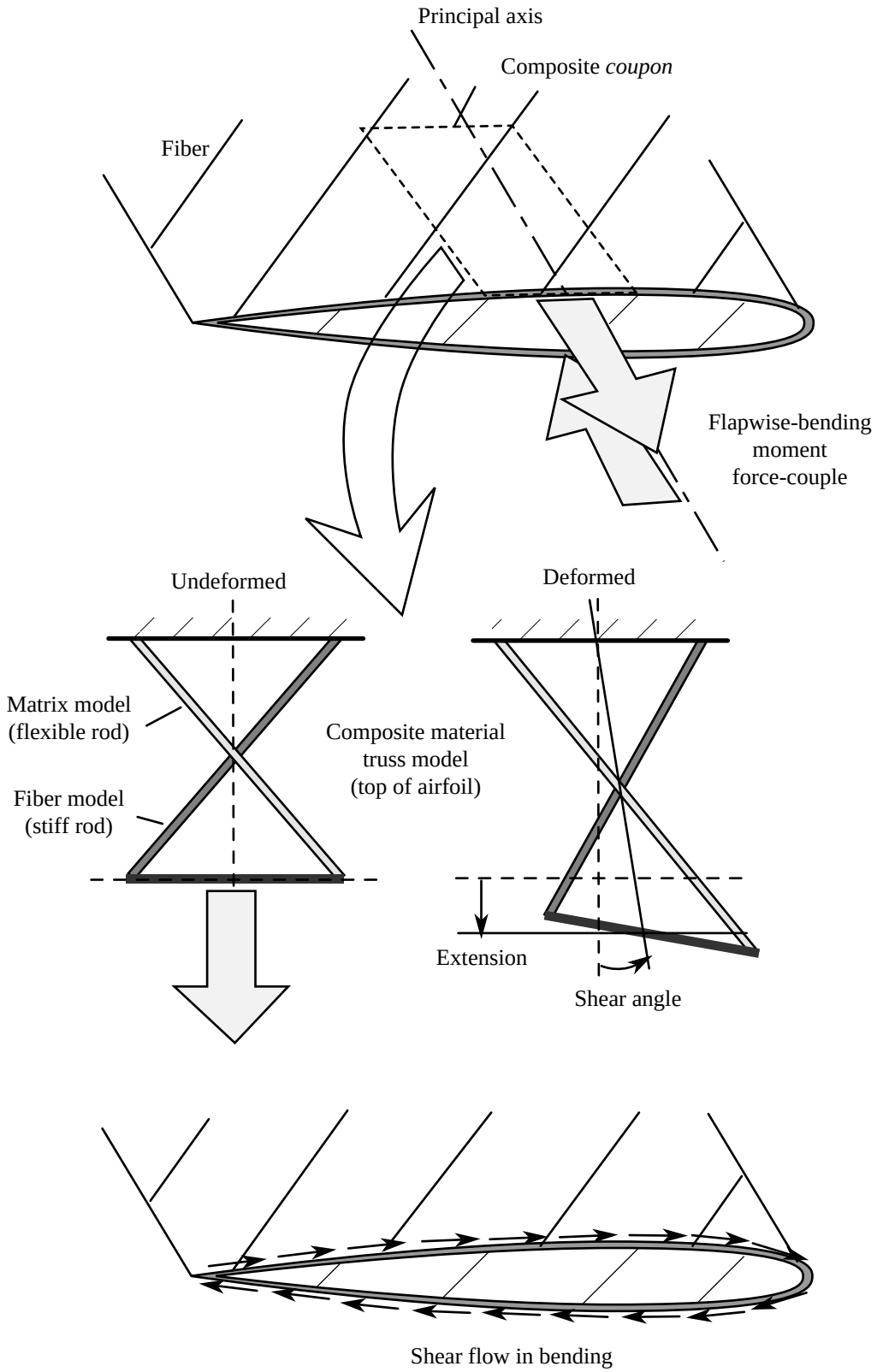

Figure 1. Truss analogy used to explain the formation of elastic bending-twist coupling in composite rotor blades with off-axis plies in a symmetric configuration.

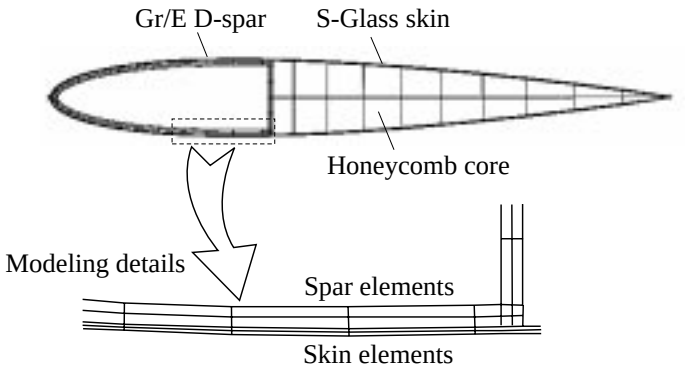

(a) Cross-section model used for baseline designs 1 and 2.

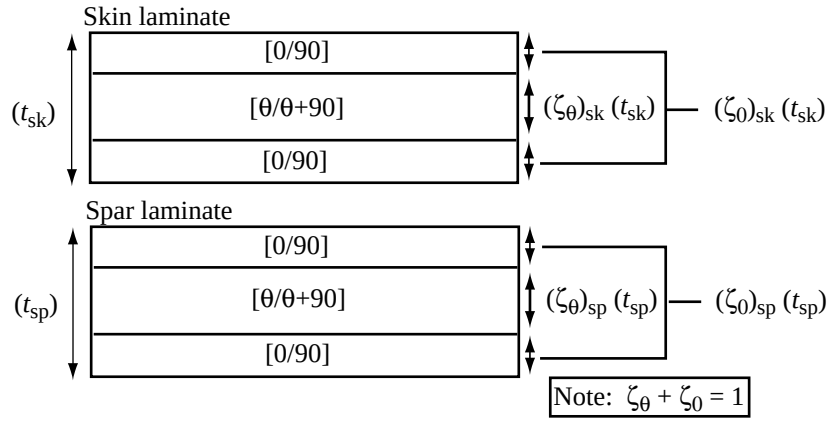

(b) Skin and spar laminate design employed in baseline blade 1 in nondimensional parameters.

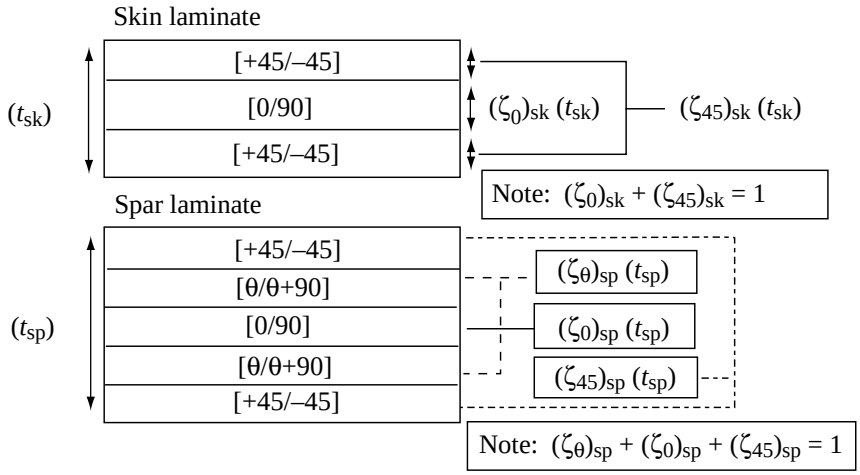

(c) Skin and spar laminate design employed in baseline blade 2 in nondimensional parameters.

Figure 2. Skin and spar laminate designs.

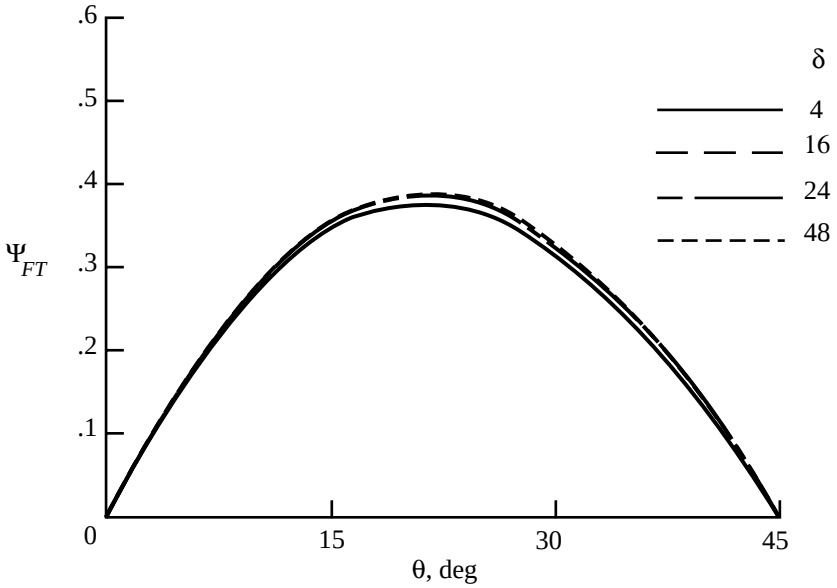

Figure 3. Flapwise-bending-twist coupling parameter as a function of ply angle for various chordwise divisions.

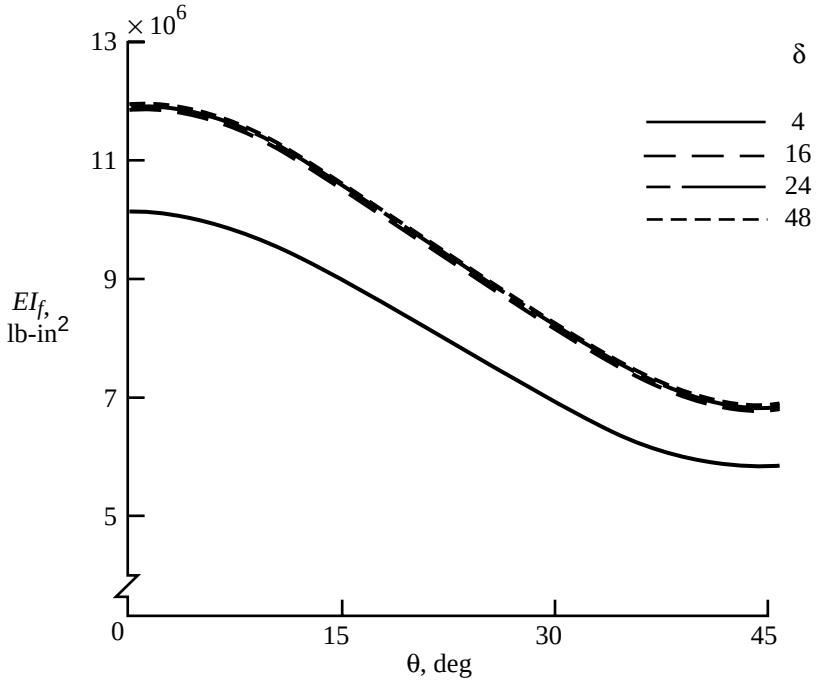

Figure 4. Flapwise stiffness as a function of ply angle for various chordwise divisions.

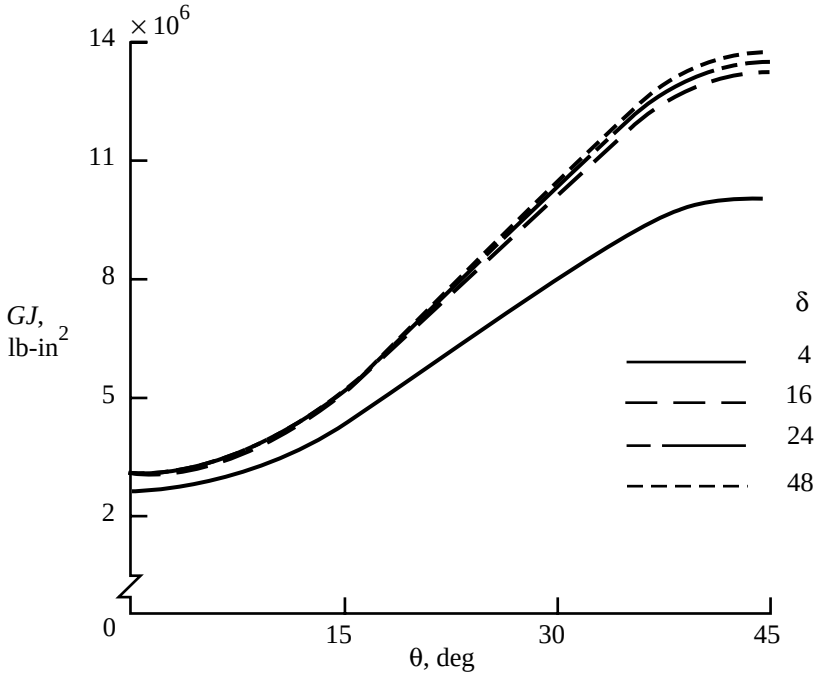

Figure 5. Torsional stiffness as a function of ply angle for various chordwise divisions.

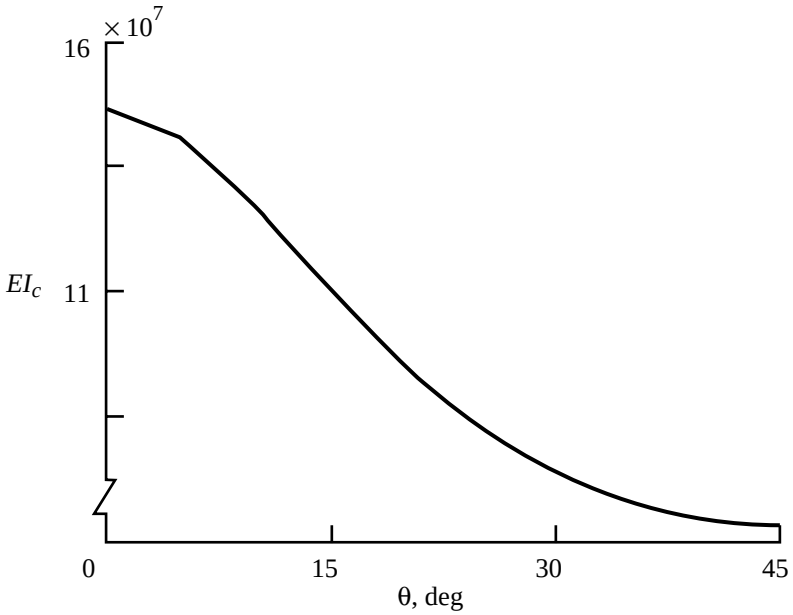

Figure 6. Chordwise stiffness as a function of ply angle for baseline design 1 blade with symmetric laminate construction.

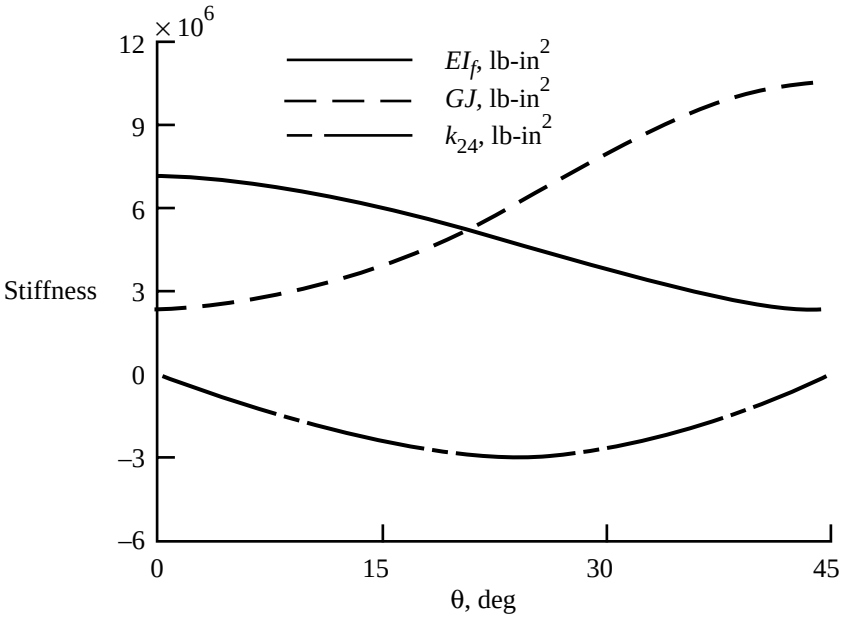

Figure 7. Flapwise, torsion, and flapwise-bending-twist-coupled stiffnesses as a function of ply angle of the baseline blade with symmetric laminate construction.

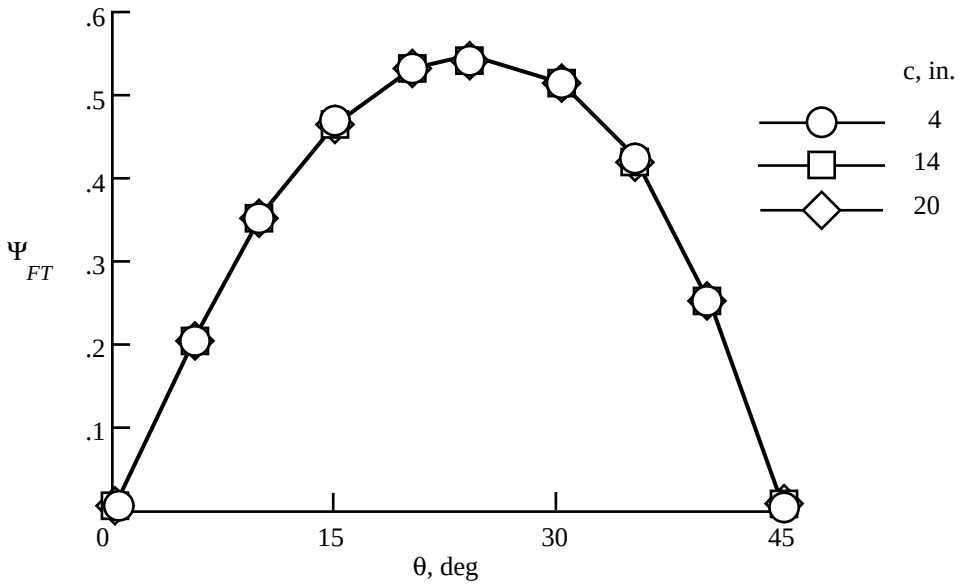

Figure 8. Bending-twist coupling parameter as a function of ply angle for several chord lengths of the baseline 1 blade with symmetric laminate construction.

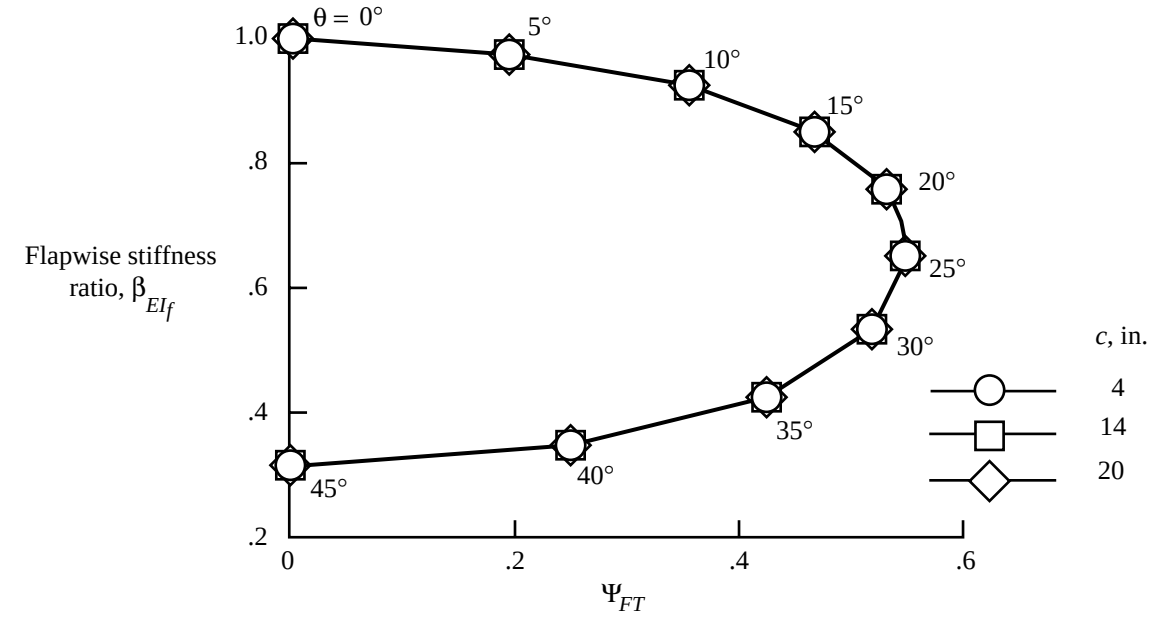

Figure 9. Flapwise-bending stiffness ratio as a function of flapwise-bending-twist coupling parameter for several chord lengths of the baseline 1 blade with symmetric laminate construction.

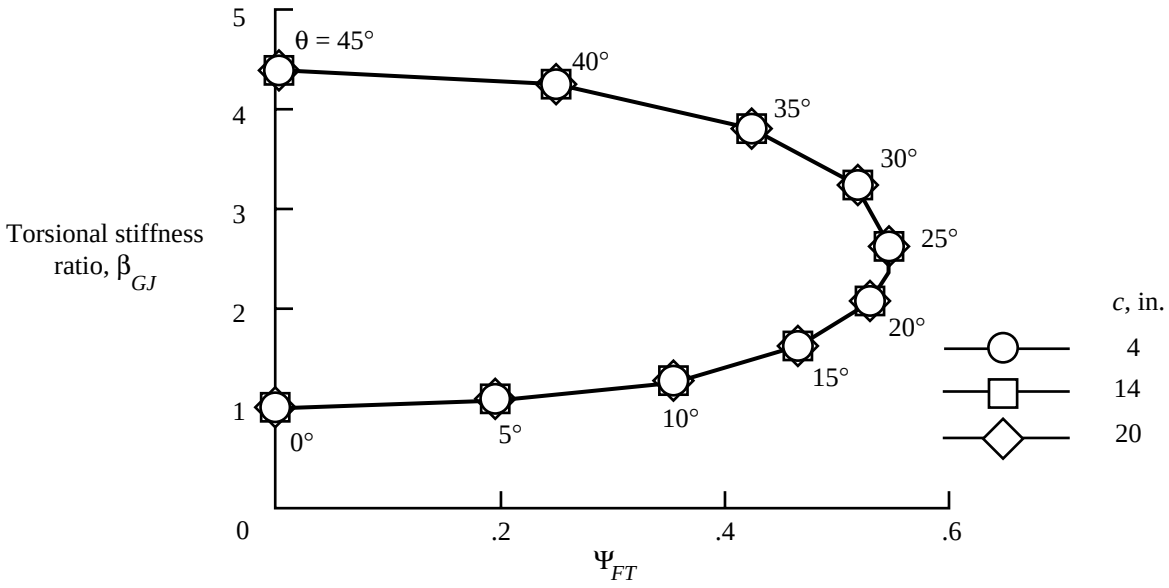

Figure 10. Torsional stiffness ratio as a function of flapwise-bending-twist coupling parameter for several chord lengths of the baseline 1 blade with symmetric laminate construction.

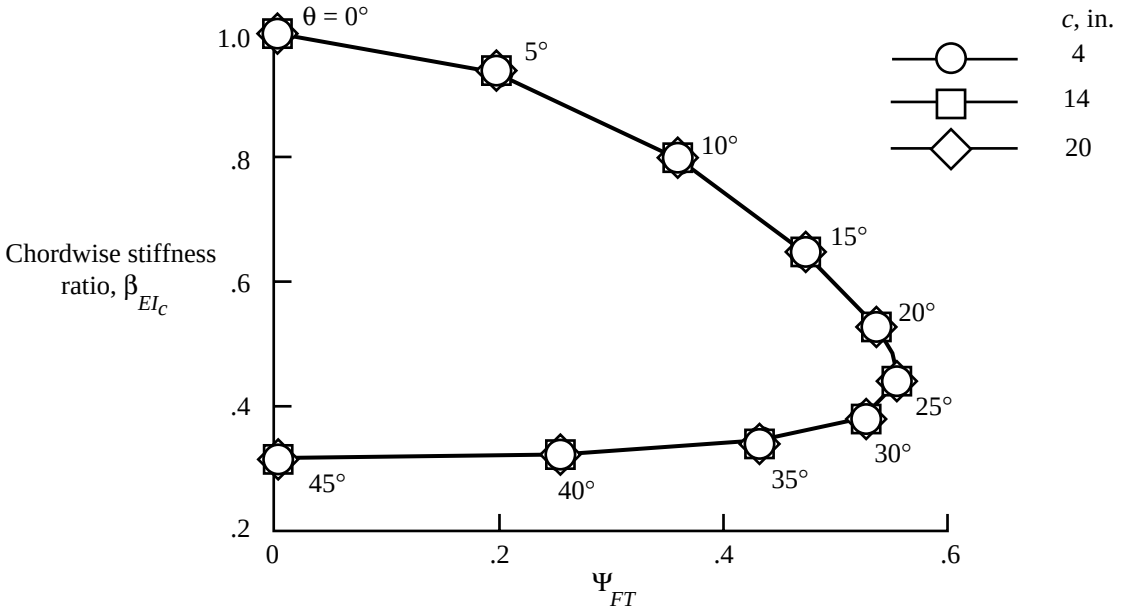

Figure 11. Chordwise-bending stiffness ratio as a function of flapwise-bending-twist coupling parameter for several chord lengths of the baseline 1 blade with symmetric laminate construction.

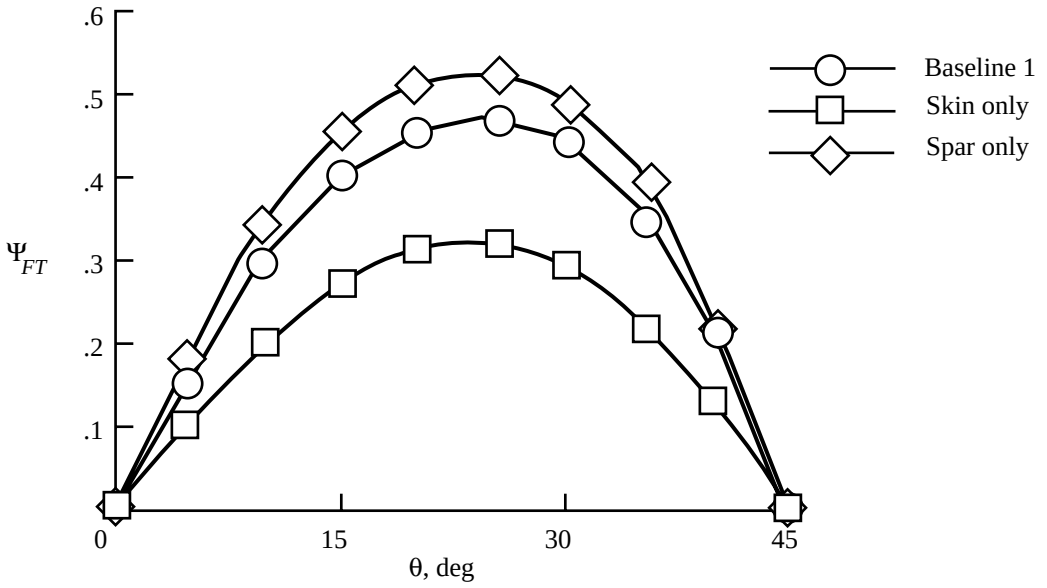

Figure 12. Contributions of the skin and spar to the flapwise-bending-twist coupling parameter as a function of ply angle.

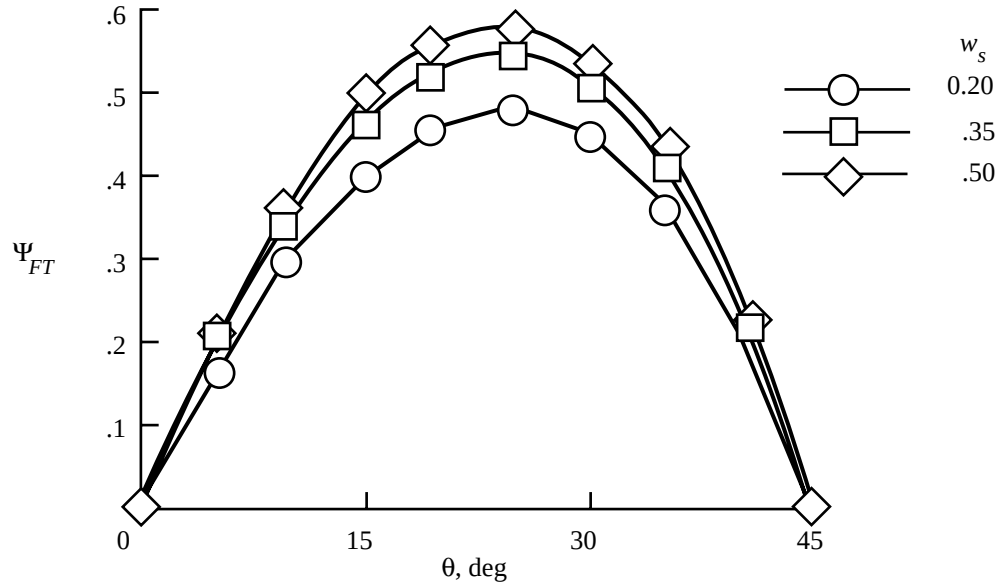

Figure 13. Flapwise-bending-twist coupling parameter as a function of ply angle for several variations of spar width of the baseline 1 blade with symmetric laminate construction.

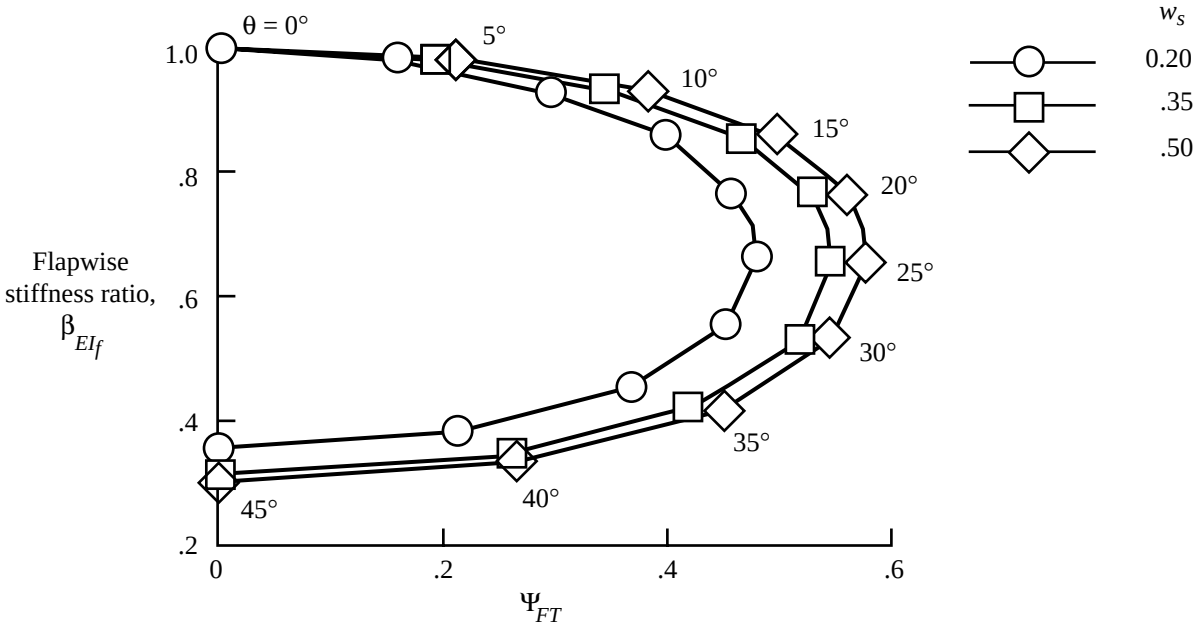

Figure 14. Flapwise-bending stiffness ratio as a function of flapwise-bending-twist coupling parameter for several variations of spar width of the baseline 1 blade with symmetric laminate construction.

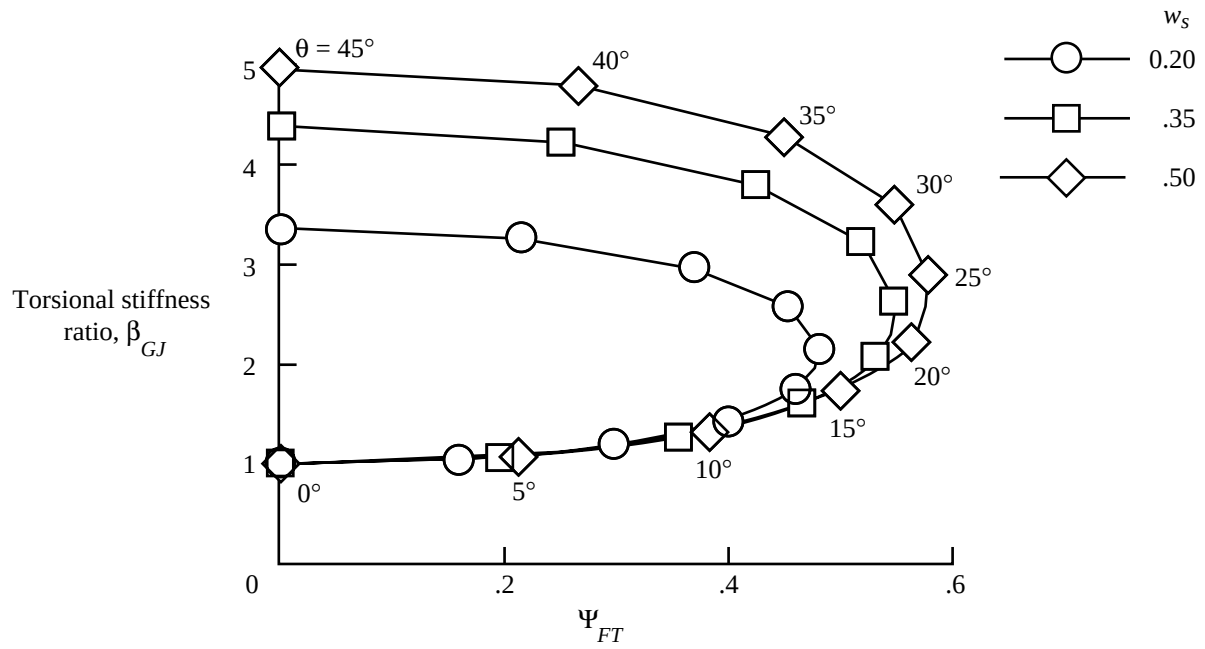

Figure 15. Torsional stiffness ratio as a function of flapwise-bending-twist coupling parameter for several variations of spar width of the baseline 1 blade with symmetric laminate construction.

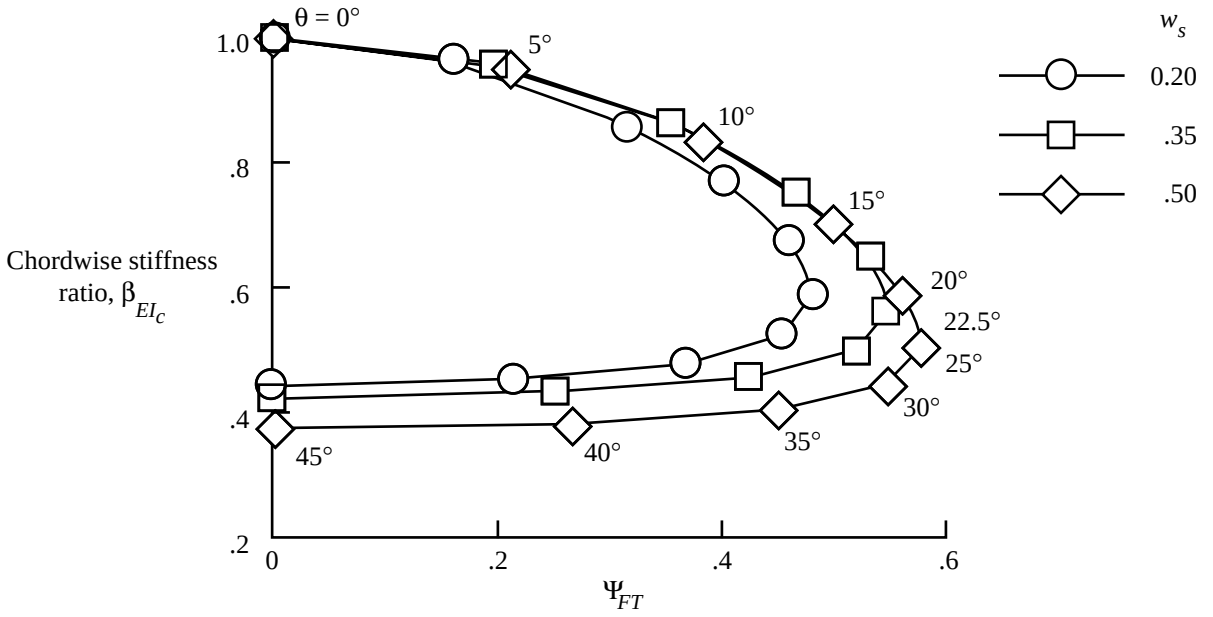

Figure 16. Chordwise-bending stiffness ratio as a function of flapwise-bending-twist coupling parameter for several variations of spar width of the baseline 1 blade with symmetric laminate construction.

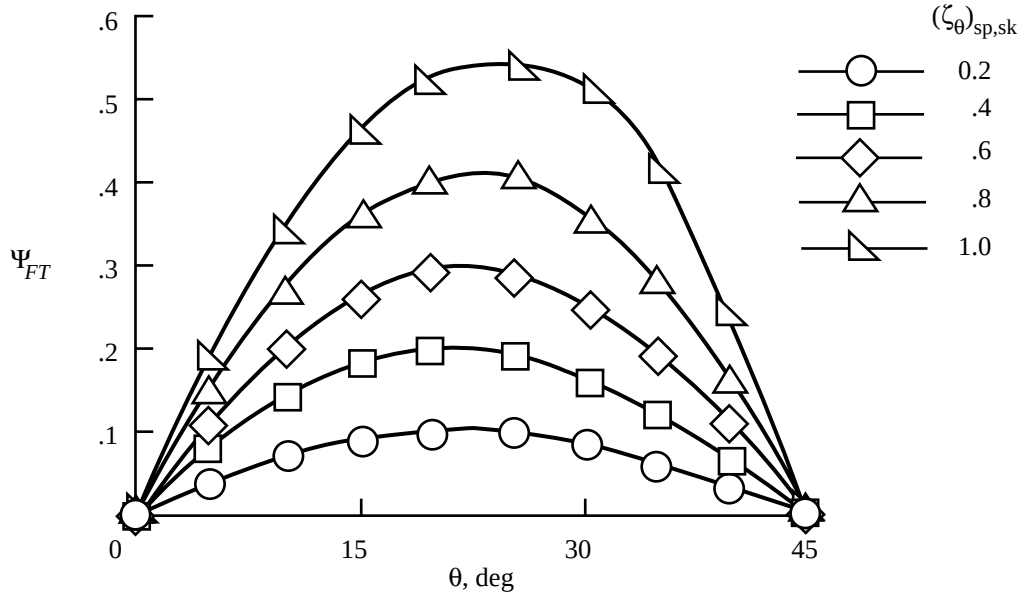

Figure 17. Flapwise-bending-twist coupling parameter as a function of ply angle for several laminate variations of the baseline 1 blade with symmetric laminate construction.

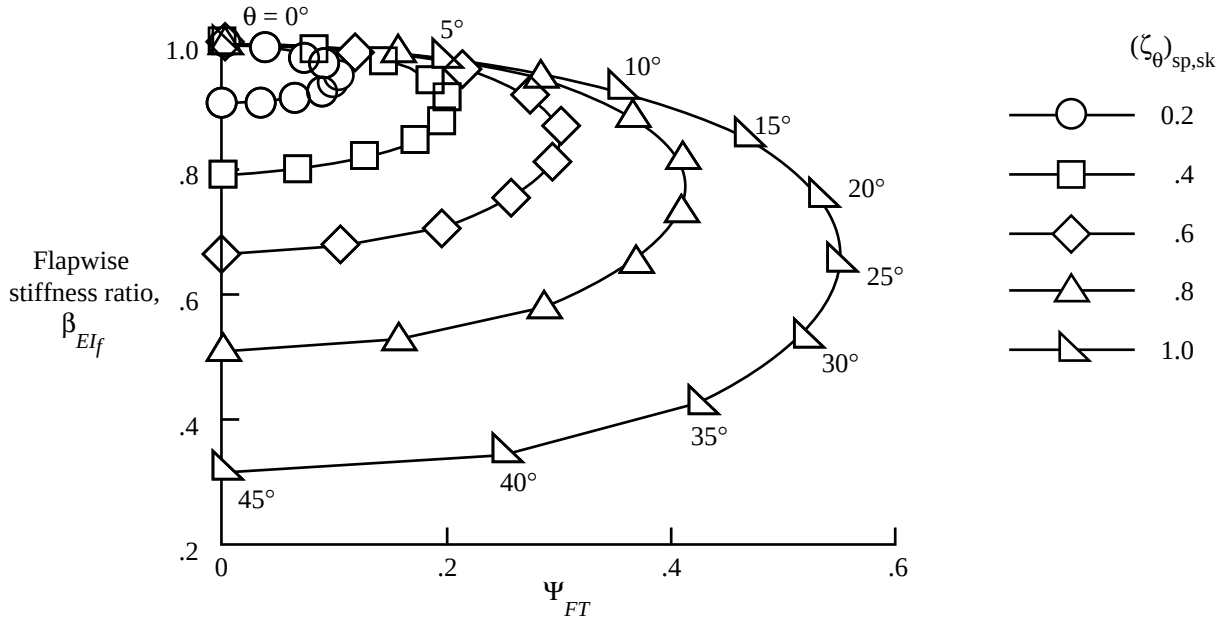

Figure 18. Flapwise-bending stiffness ratio as a function of flapwise-bending-twist coupling parameter for several laminate variations of the baseline 1 blade with symmetric laminate construction.

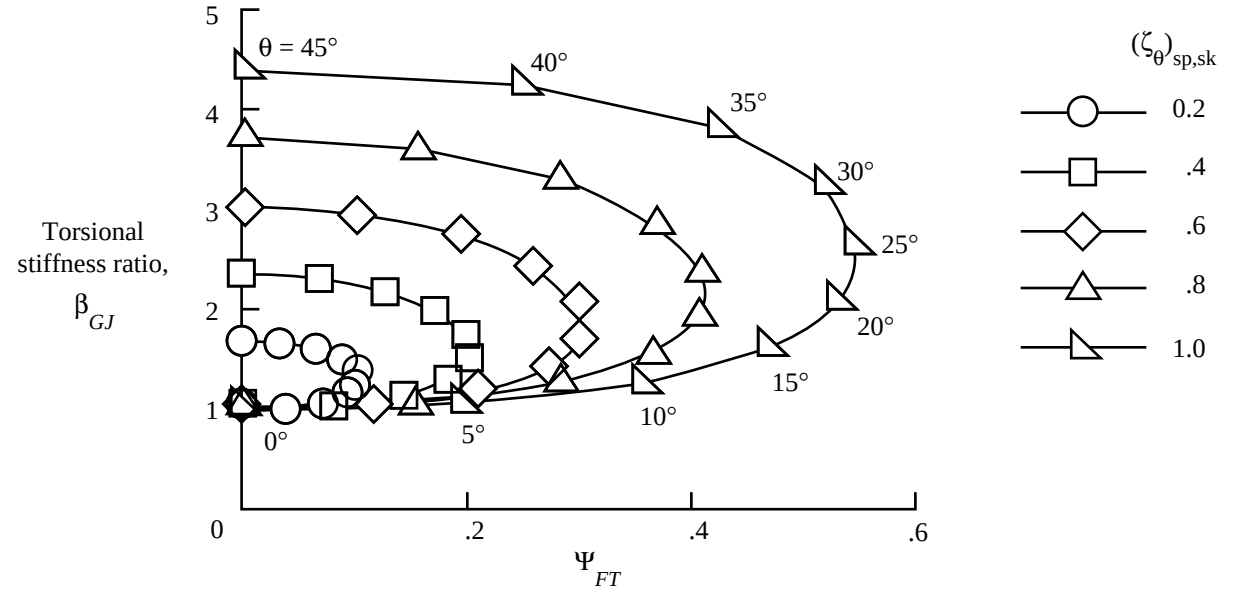

Figure 19. Torsional stiffness ratio as a function of flapwise-bending-twist coupling parameter for several laminate variations of the baseline 1 blade with symmetric laminate construction.

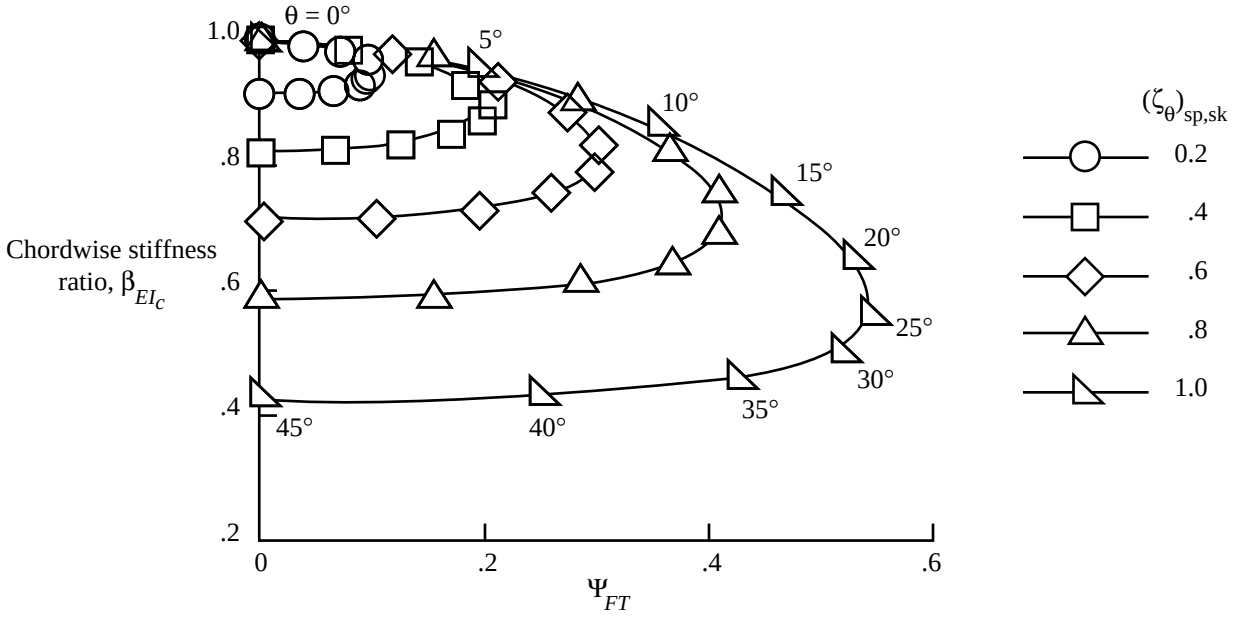

Figure 20. Chordwise-bending stiffness ratio as a function of flapwise-bending-twist coupling parameter for several laminate variations of the baseline 1 blade with symmetric laminate construction.

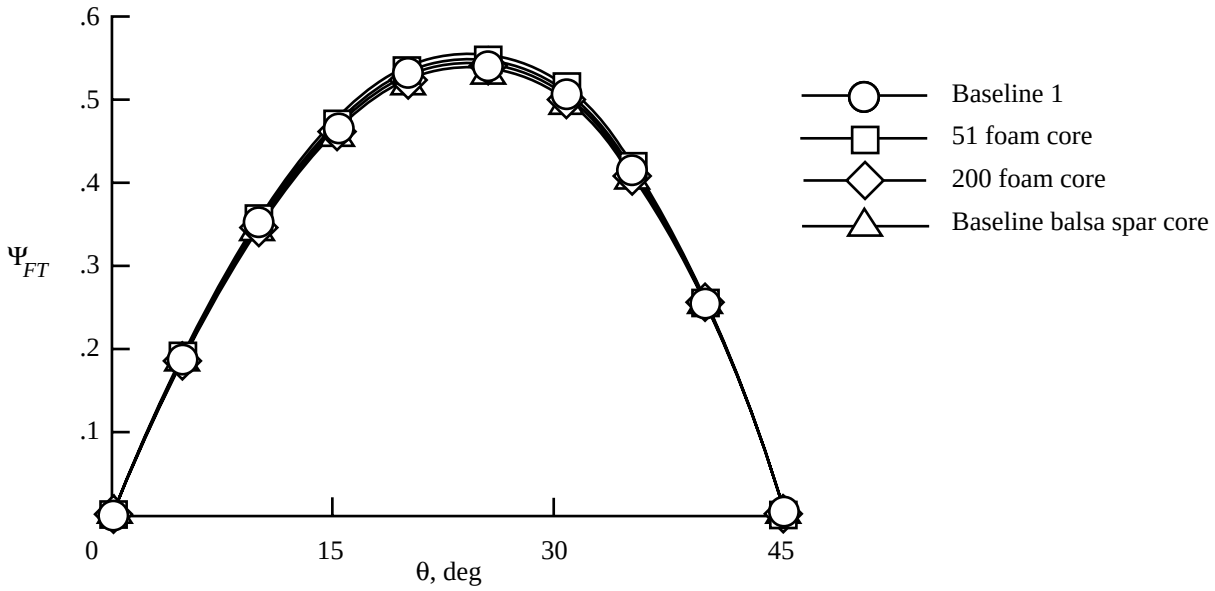

Figure 21. Flapwise-bending-twist coupling parameter as a function of ply angle for several variations of the baseline 1 core material.

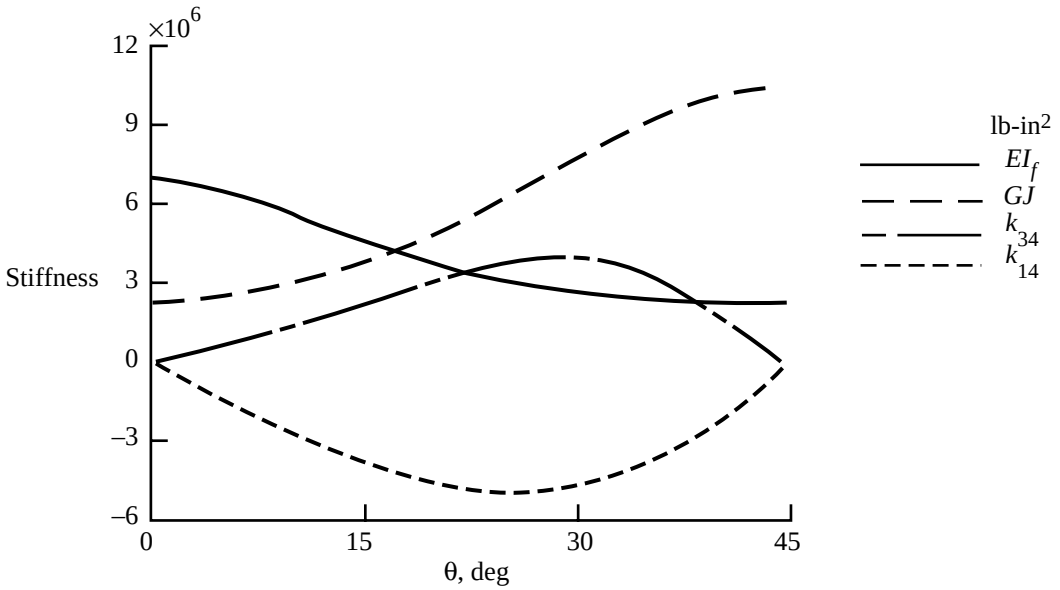

Figure 22. Flapwise, torsion, extension-twist, and chordwise-bending-twist stiffnesses as a function of ply angle for the baseline 1 blade with antisymmetric laminate construction.

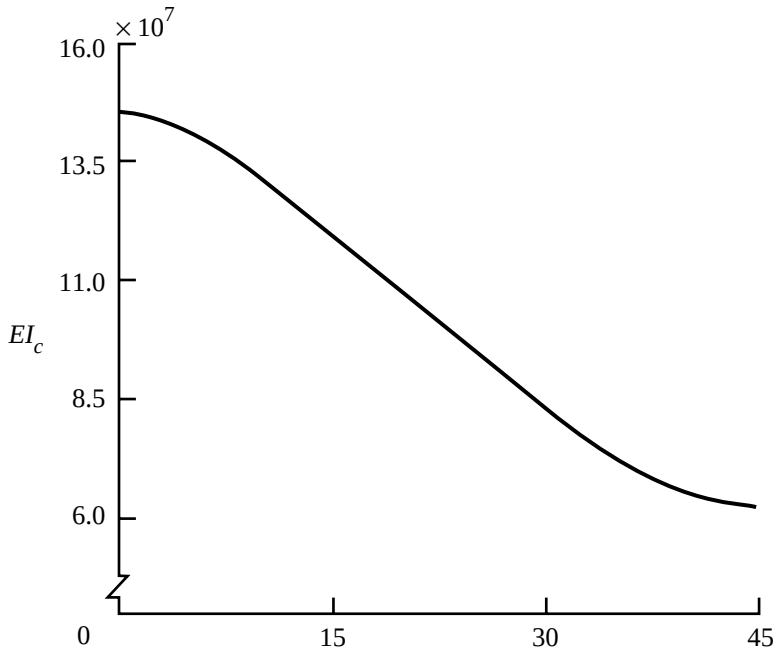

Figure 23. Chordwise bending stiffness as a function of ply angle for the baseline 1 blade with antisymmetric laminate construction.

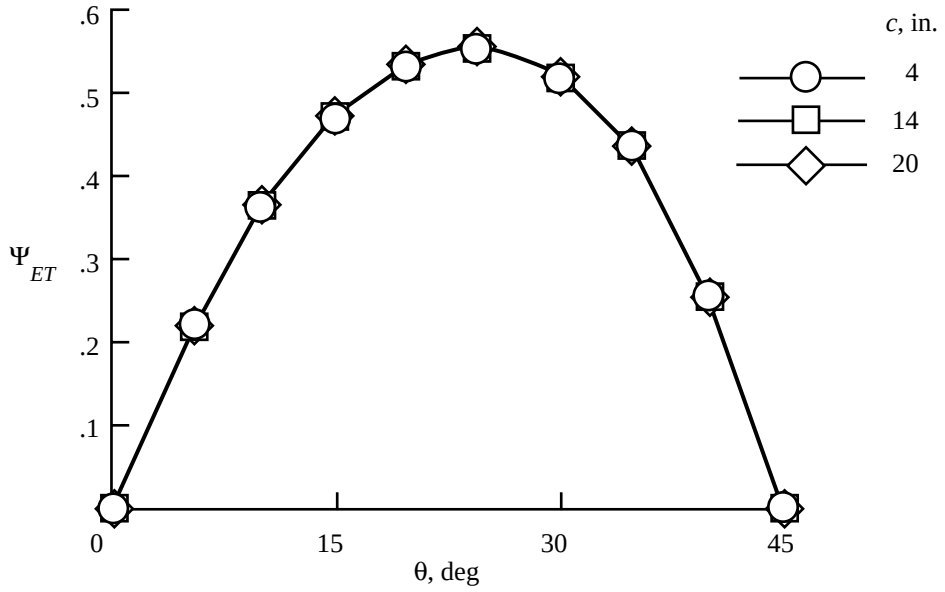

Figure 24. Extension-twist-coupled stiffness parameter as a function of ply angle for several chord lengths of the baseline 1 blade with antisymmetric laminate construction.

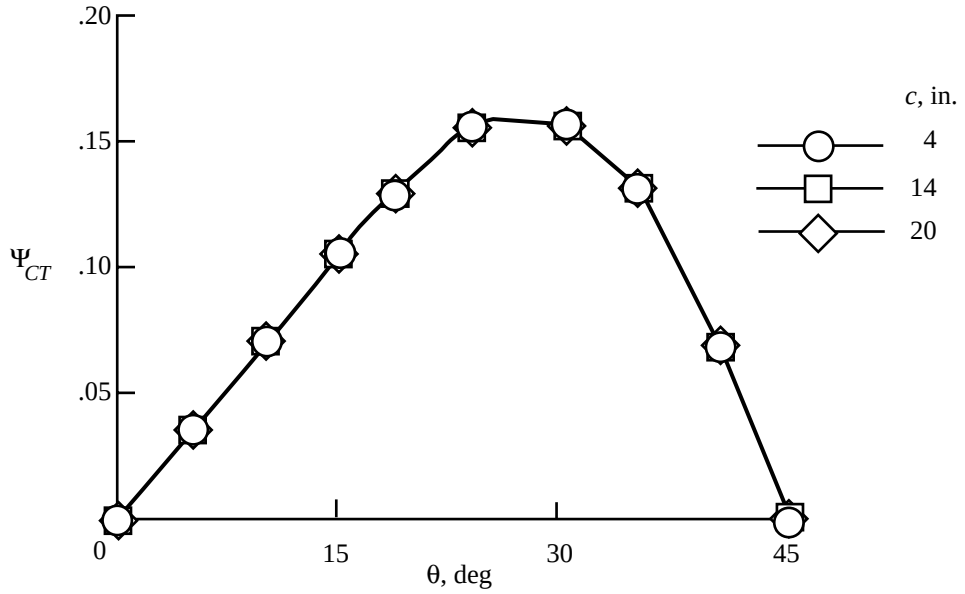

Figure 25. Chordwise-bending-twist-coupled stiffness parameter as a function of ply angle for several chord lengths of the baseline 1 blade with antisymmetric laminate construction.

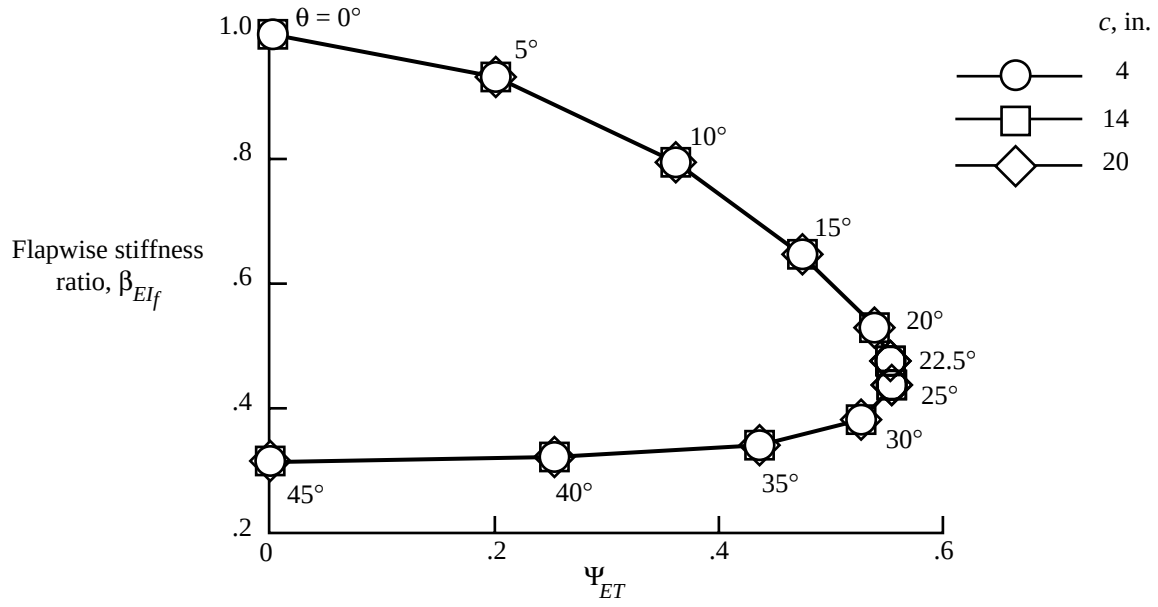

Figure 26. Flapwise-bending stiffness ratio as a function of extension-twist coupling parameter for several chord lengths of the baseline 1 blade with antisymmetric laminate construction.

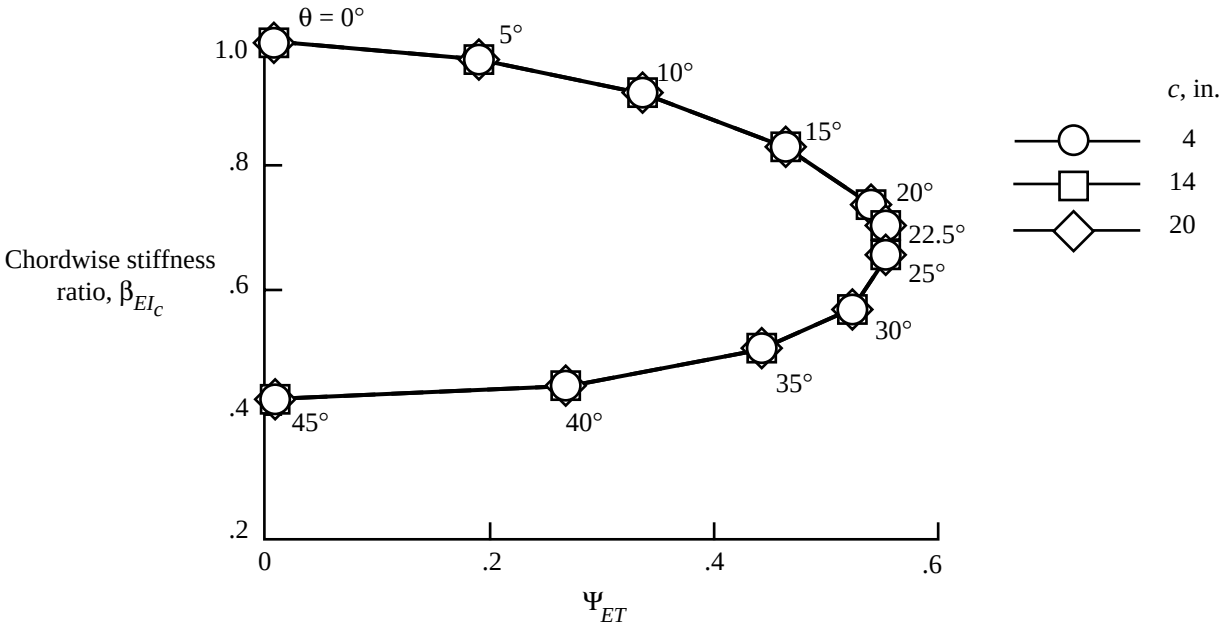

Figure 27. Chordwise-bending stiffness ratio as a function of extension-twist coupling parameter for several chord lengths of the baseline 1 blade with antisymmetric laminate construction.

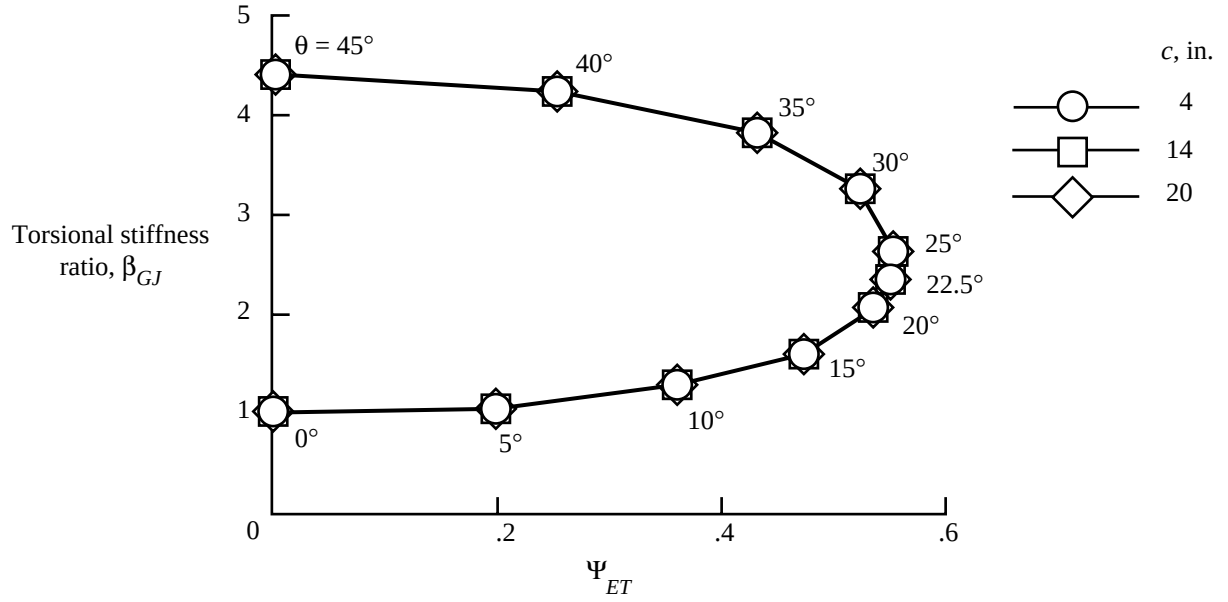

Figure 28. Torsional stiffness ratio as a function of extension-twist coupling parameter for several chord lengths of the baseline 1 blade with antisymmetric laminate construction.

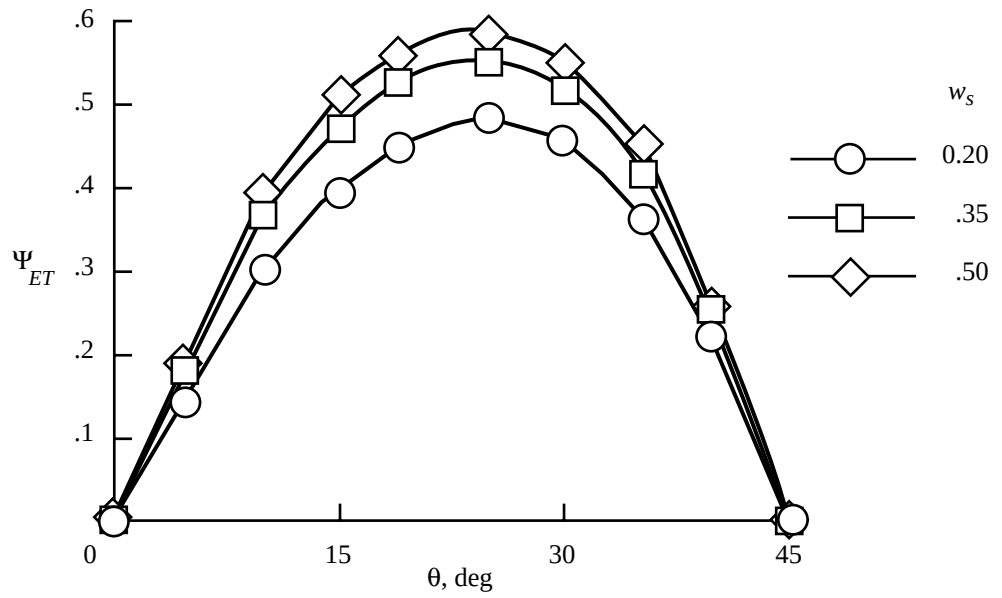

Figure 29. Extension-twist coupling parameter as a function of ply angle for several variations of spar width of the baseline 1 blade with antisymmetric laminate construction.

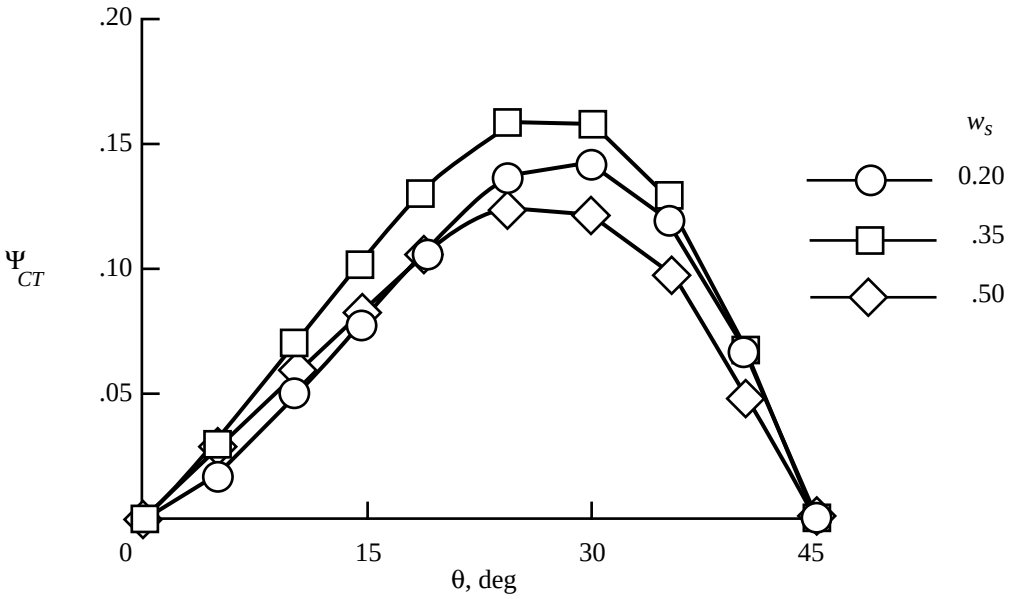

Figure 30. Chordwise-bending-twist coupling parameter as a function of ply angle for several variations of spar width of the baseline 1 blade with antisymmetric laminate construction.

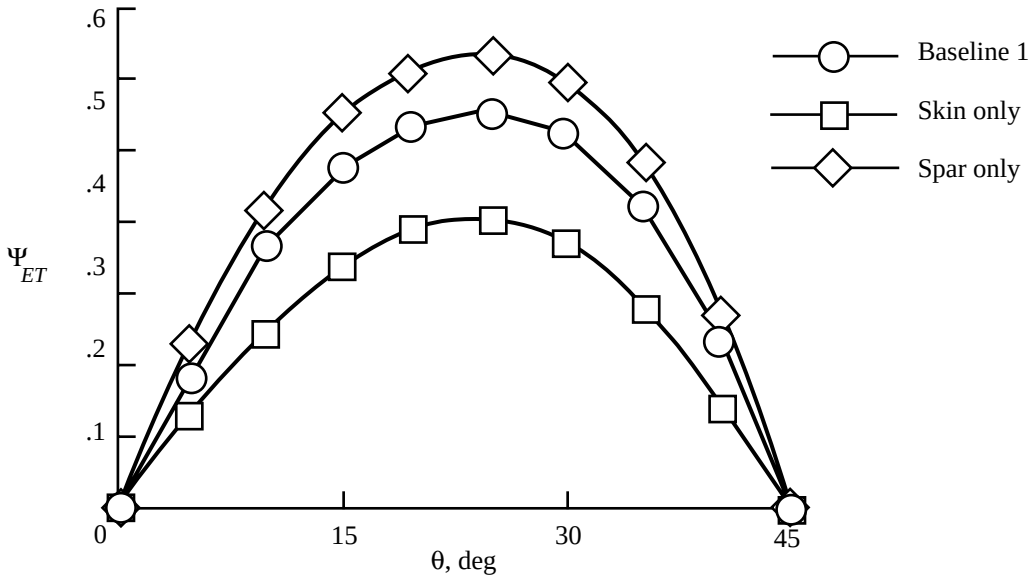

Figure 31. Extension-twist coupling parameter as a function of ply angle for several variations of the baseline 1 blade with antisymmetric laminate construction.

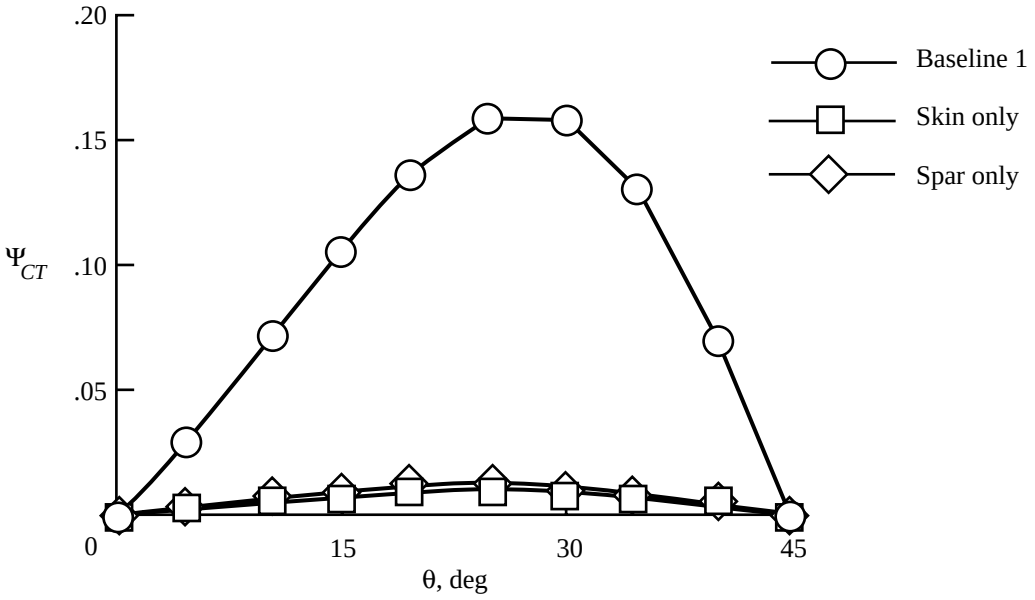

Figure 32. Chordwise-bending-twist coupling parameter as a function of ply angle for several variations of the baseline 1 blade with antisymmetric laminate construction.

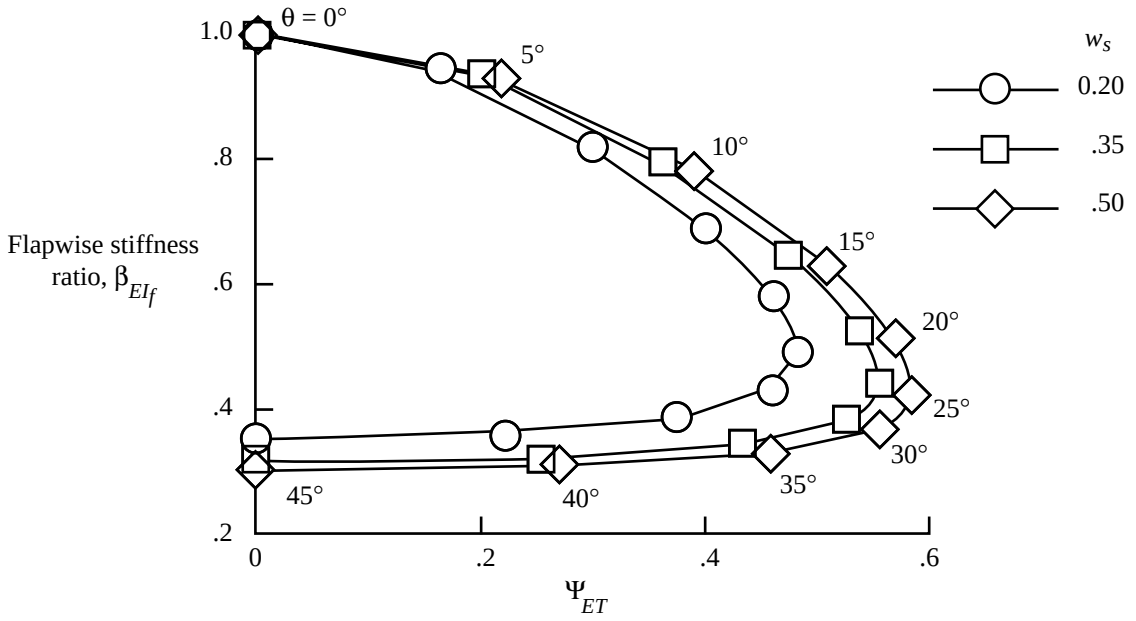

Figure 33. Flapwise-bending stiffness ratio as a function of flapwise-bending-twist coupling parameter for several variations of spar width of the baseline 1 blade with antisymmetric laminate construction.

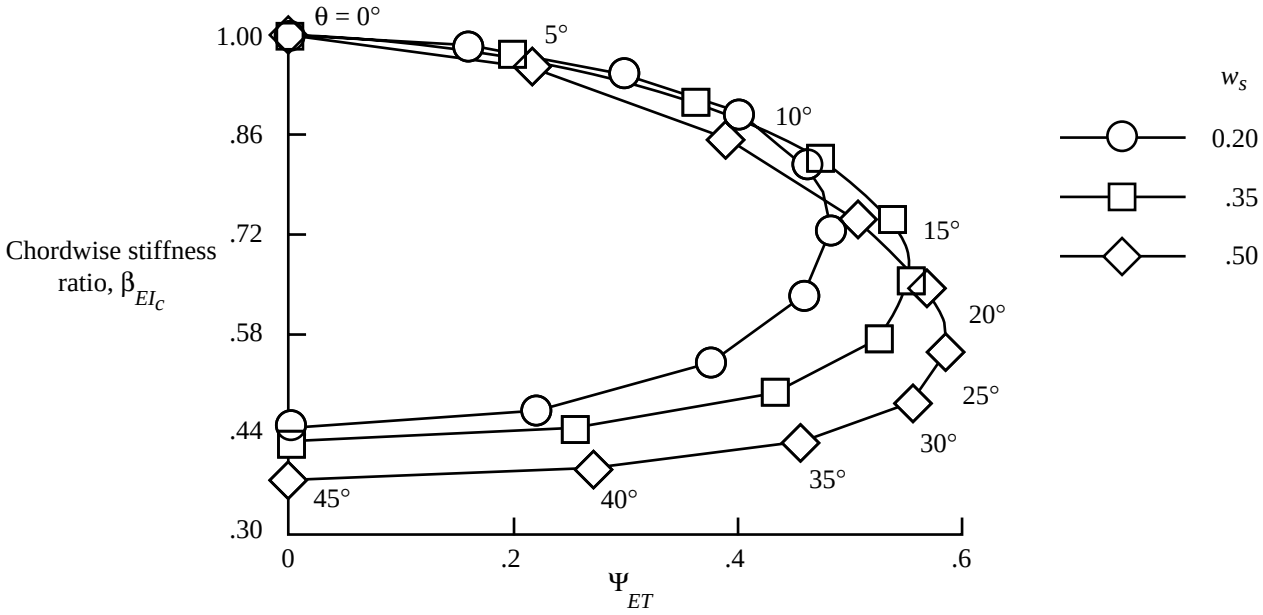

Figure 34. Chordwise-bending stiffness ratio as a function of flapwise-bending-twist coupling parameter for several variations of spar width of the baseline 1 blade with antisymmetric laminate construction.

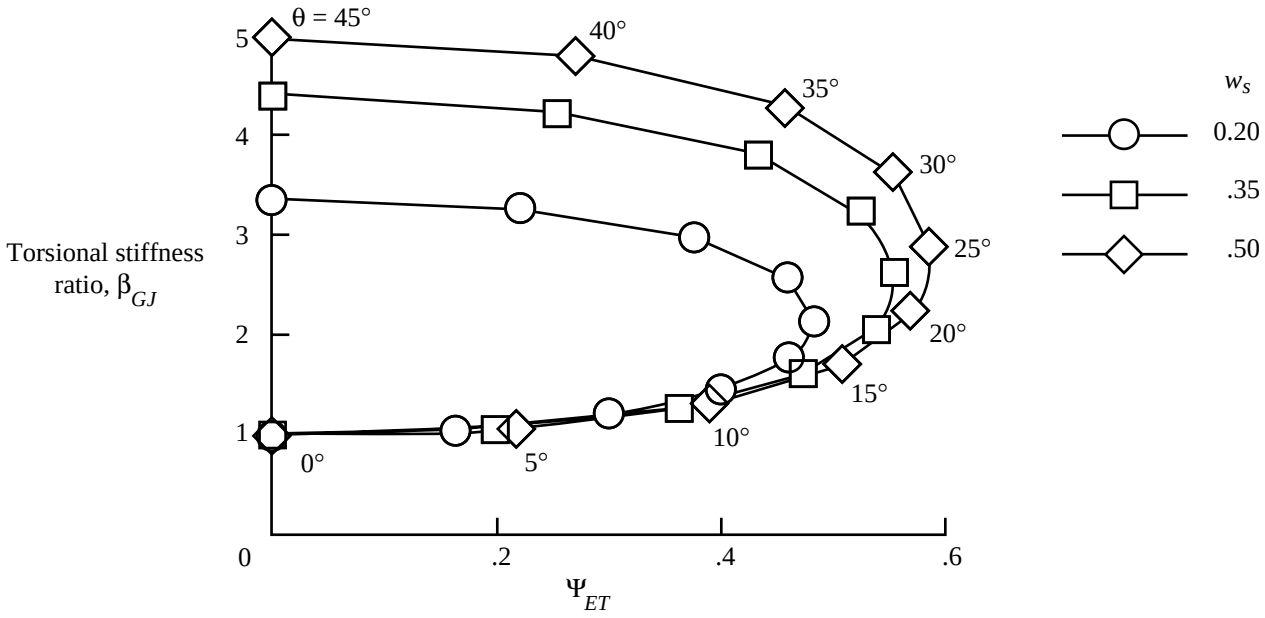

Figure 35. Torsional stiffness ratio as a function of flapwise-bending-twist coupling parameter for several variations of spar width of the baseline 1 blade with antisymmetric laminate construction.

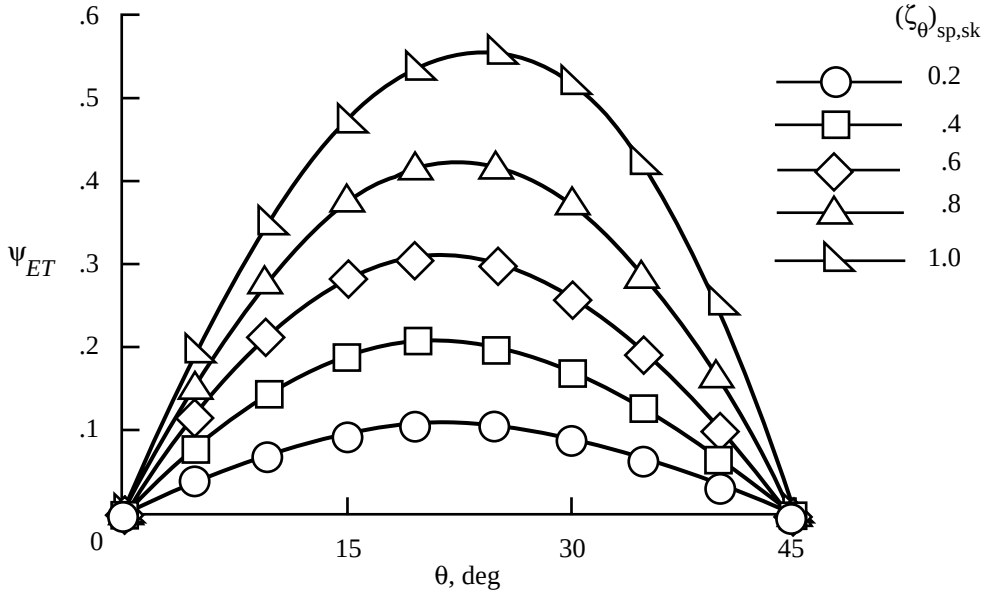

Figure 36. Extension-twist coupling parameter as a function of ply angle for several laminate variations of the baseline 1 blade with antisymmetric laminate construction.

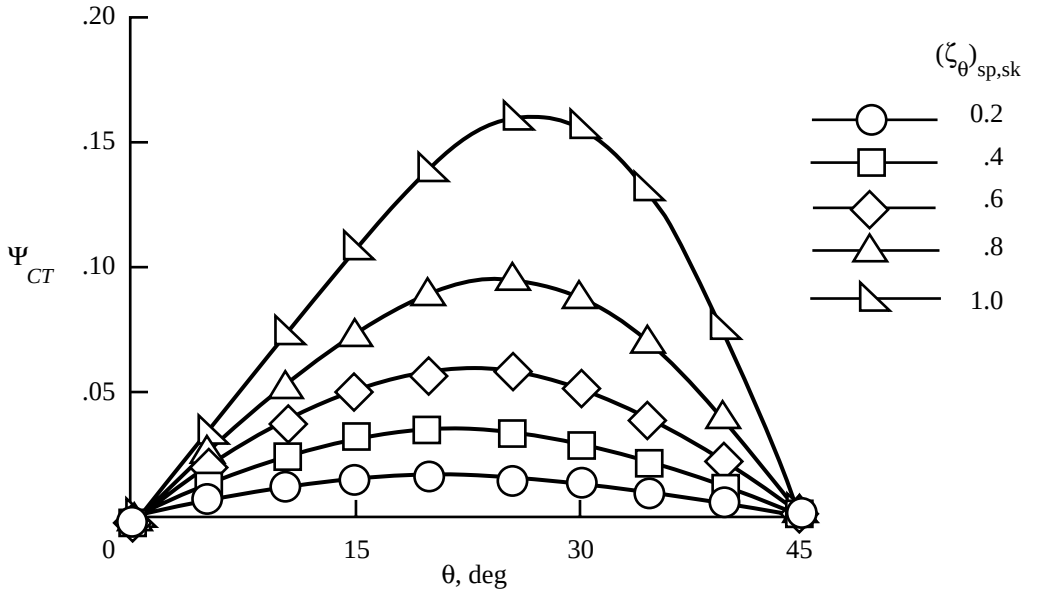

Figure 37. Chordwise-bending-twist coupling parameter as a function of ply angle for several laminate variations of the baseline 1 blade with antisymmetric laminate construction.

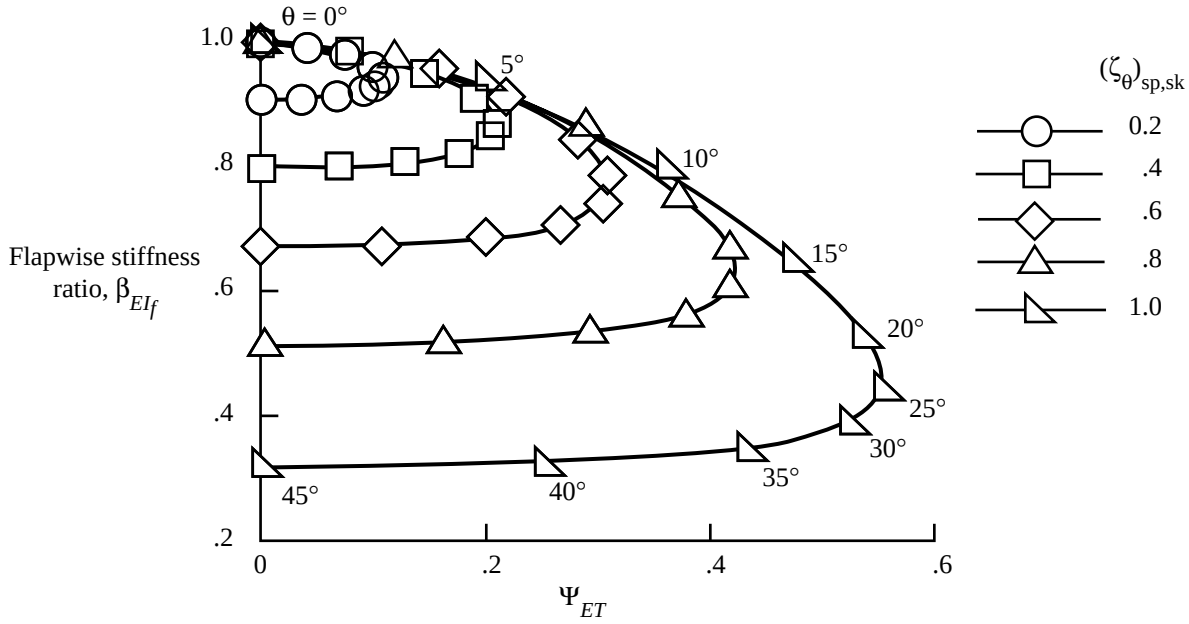

Figure 38. Flapwise-bending stiffness ratio as a function of extension-twist coupling parameter for several laminate variations of the baseline 1 blade with antisymmetric laminate construction.

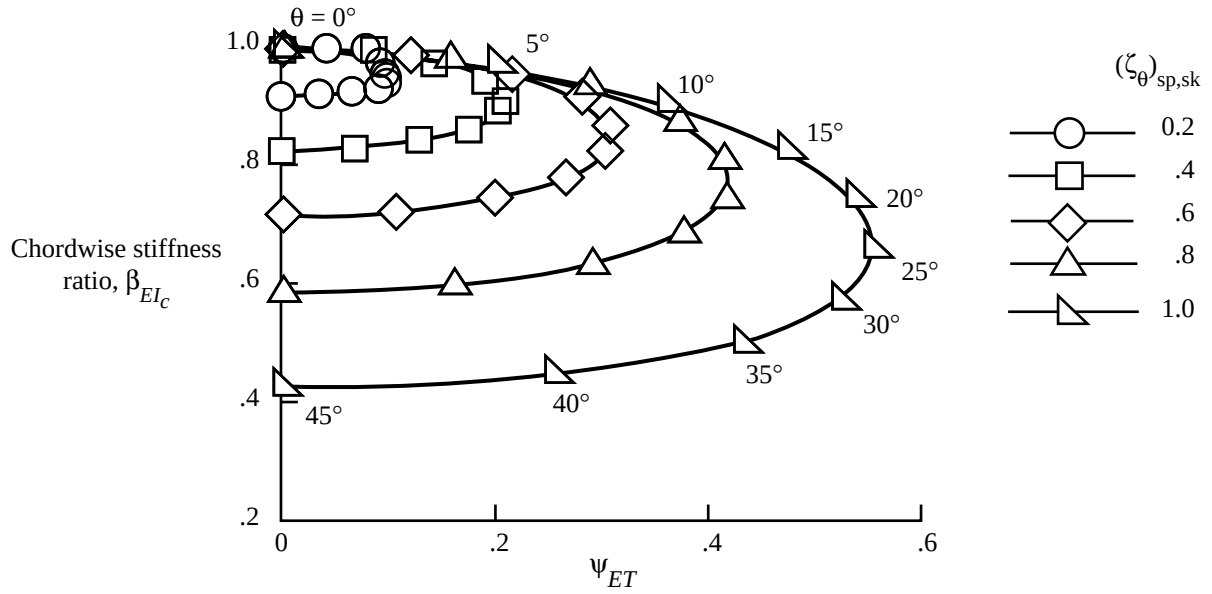

Figure 39. Chordwise-bending stiffness ratio as a function of extension-twist coupling parameter for several laminate variations of the baseline 1 blade with antisymmetric laminate construction.

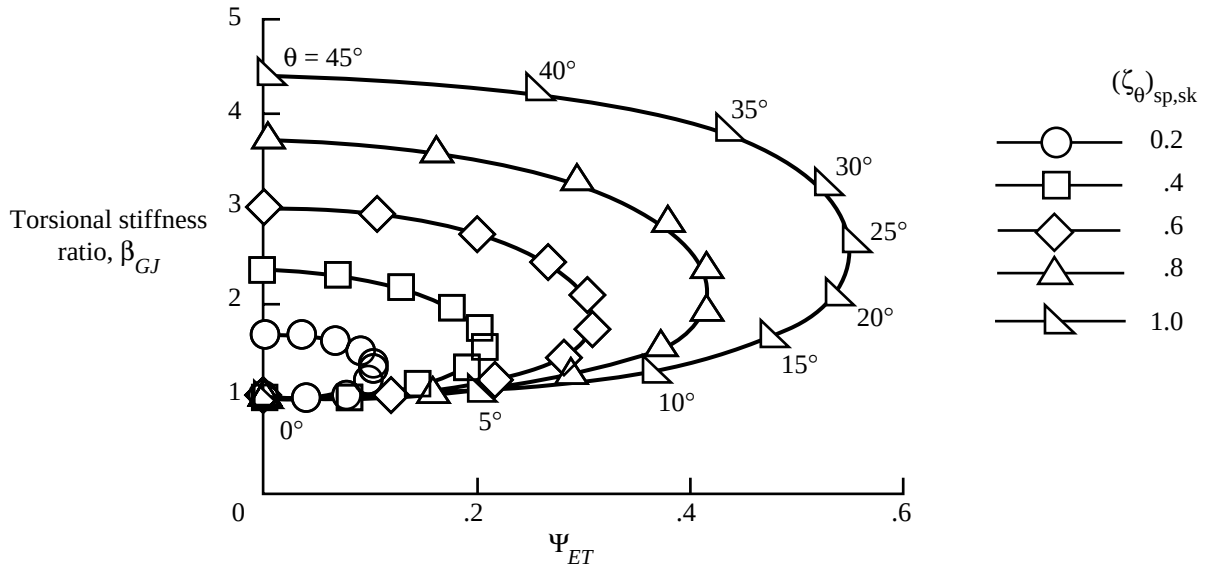

Figure 40. Torsional stiffness ratio as a function of extension-twist coupling parameter for several laminate variations of the baseline 1 blade with antisymmetric laminate construction.

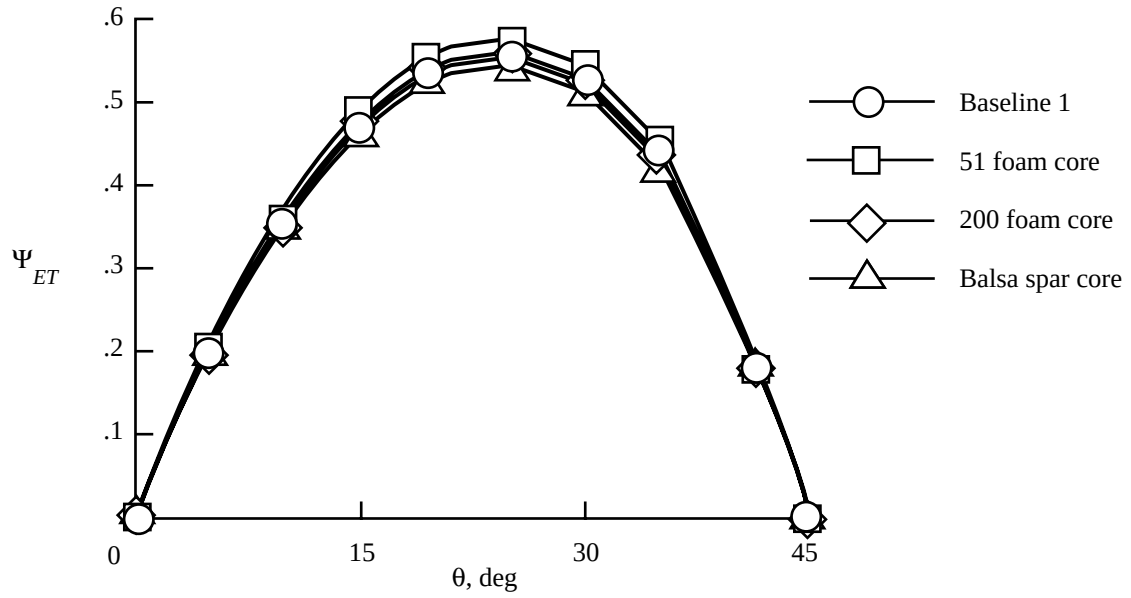

Figure 41. Extension-twist coupling parameter as a function of ply angle for several variations of core material of the baseline 1 with antisymmetric laminate construction.

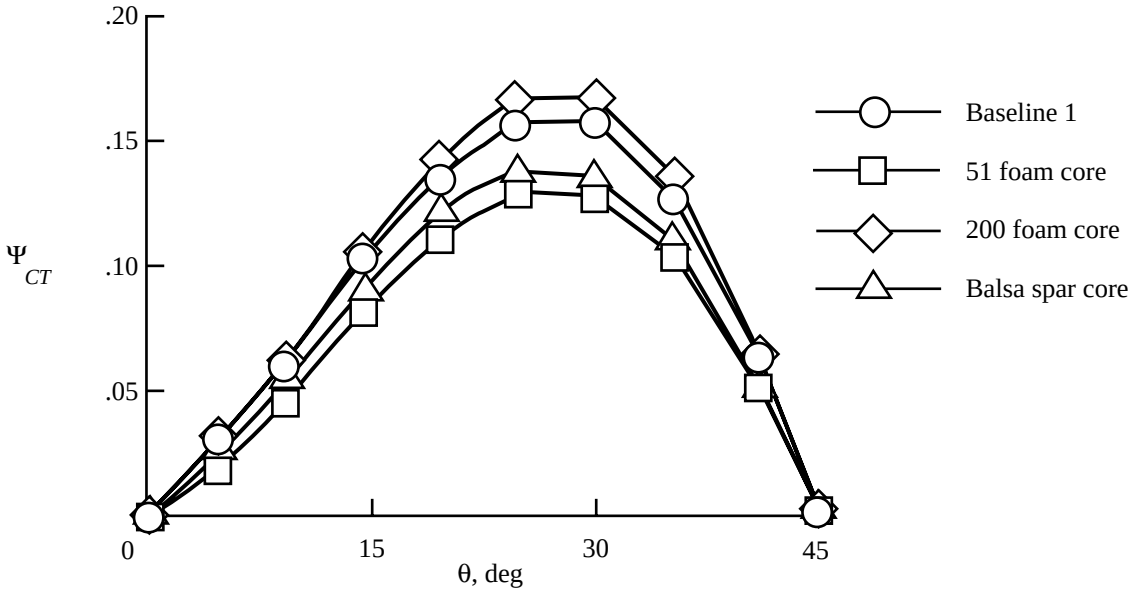

Figure 42. Chordwise-bending-twist coupling parameter as a function of ply angle for several variations of core material of the baseline 1 blade with antisymmetric laminate construction.

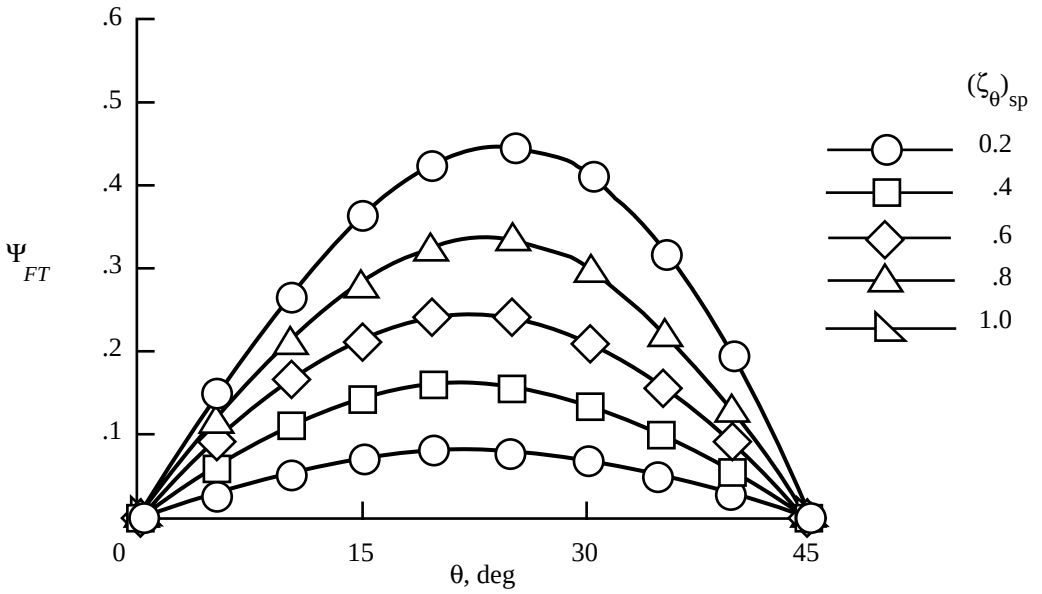

Figure 43. Flapwise-bending-twist coupling parameter as a function of ply angle for changes in $(\zeta_\theta)_{sp}$ of the baseline 2 blade with symmetric laminate construction.

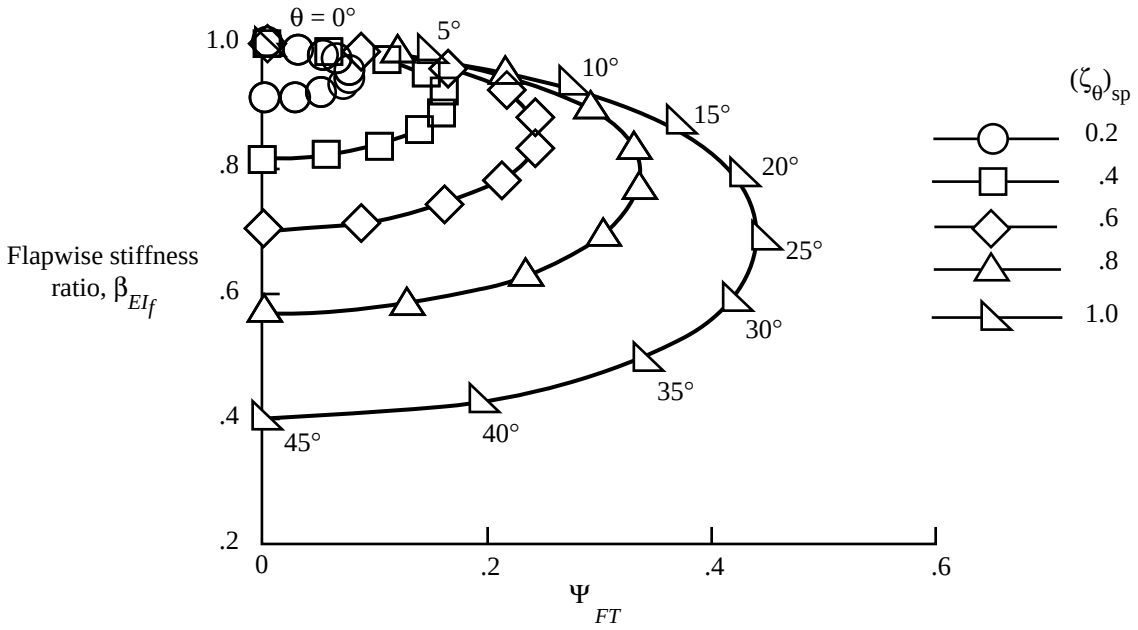

Figure 44. Flapwise-bending stiffness ratio as a function of flapwise-bending-twist coupling parameter for changes in $(\zeta_\theta)_{sp}$ of the baseline 2 blade with symmetric laminate construction.

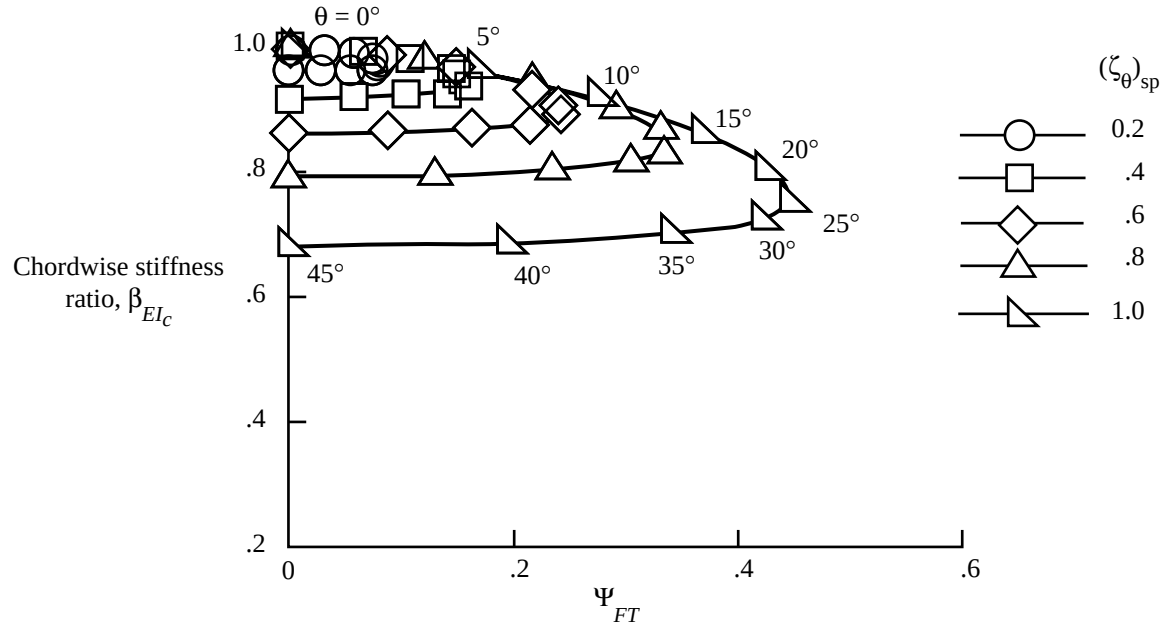

Figure 45. Chordwise-bending stiffness ratio as a function of flapwise-bending-twist coupling parameter for changes in $(\zeta_\theta)_{sp}$ of the baseline 2 blade with symmetric laminate construction.

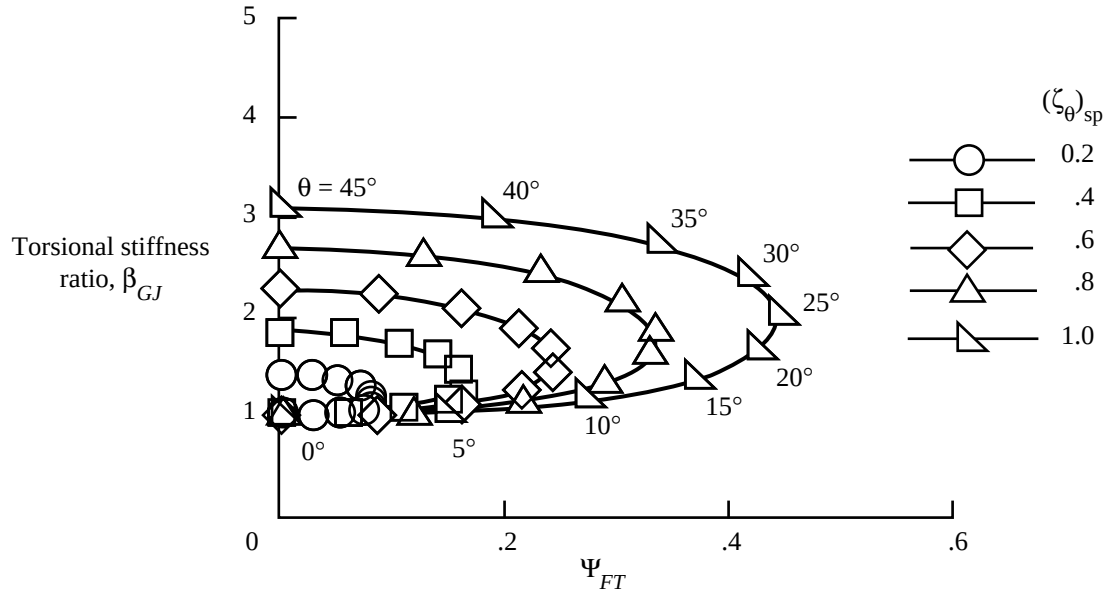

Figure 46. Torsional stiffness ratio as a function of flapwise-bending-twist coupling parameter for changes in $(\zeta_\theta)_{sp}$ of the baseline 2 blade with symmetric laminate construction.

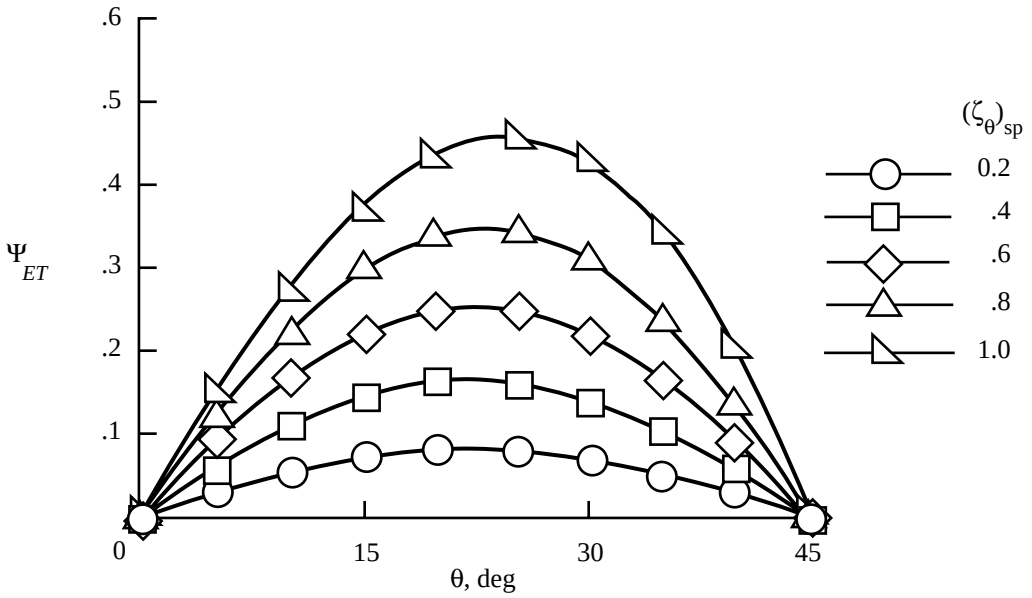

Figure 47. Extension-twist coupling parameter as a function of ply angle for changes in $(\zeta_\theta)_{\mathrm{sp}}$ of the baseline 2 blade with antisymmetric laminate construction.

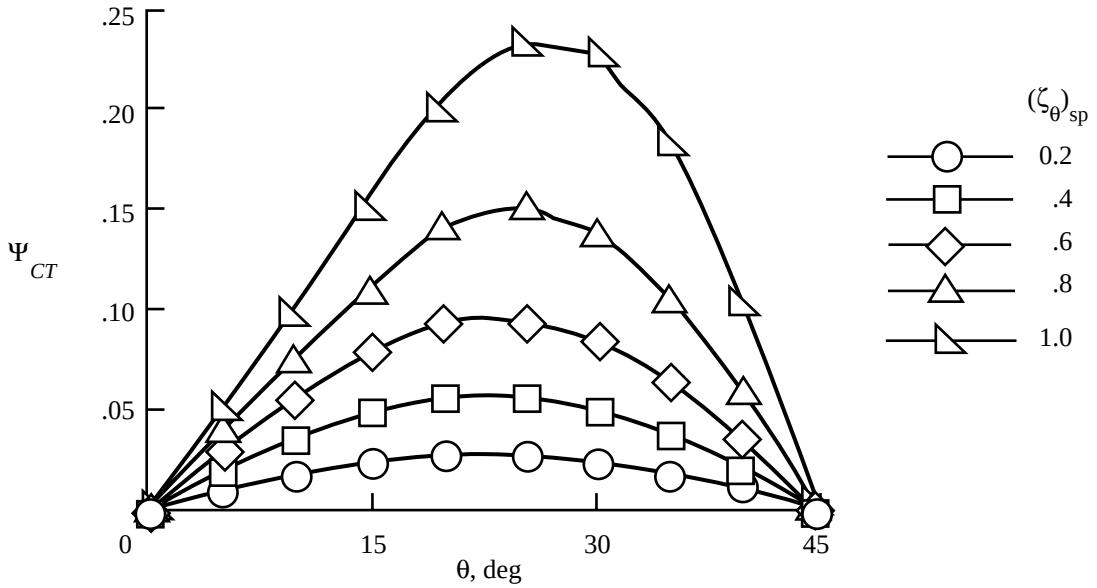

Figure 48. Chordwise-bending-twist coupling parameter as a function of ply angle for changes in $(\zeta_\theta)_{\mathrm{sp}}$ of the baseline 2 blade with antisymmetric laminate construction.

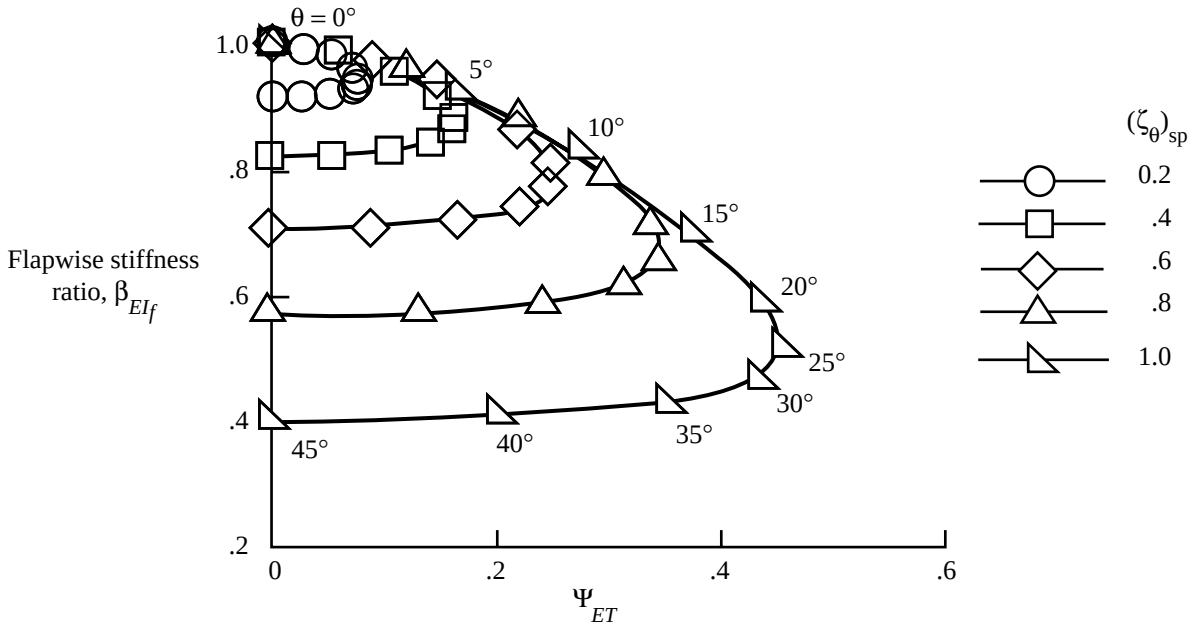

Figure 49. Flapwise-bending stiffness ratio as a function of extension-twist coupling parameter for changes in $(\zeta_\theta)_{\mathrm{sp}}$ of the baseline 2 blade with antisymmetric laminate construction.

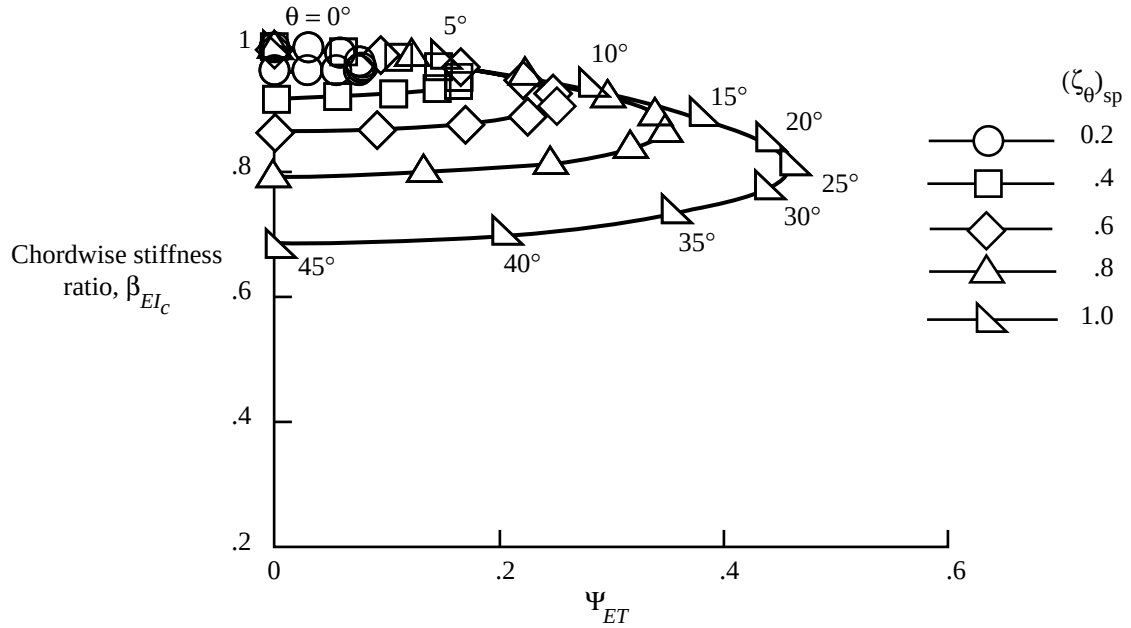

Figure 50. Chordwise-bending stiffness ratio as a function of extension-twist coupling parameter for changes in $(\zeta_\theta)_{\mathrm{sp}}$ of the baseline 2 blade with antisymmetric laminate construction.

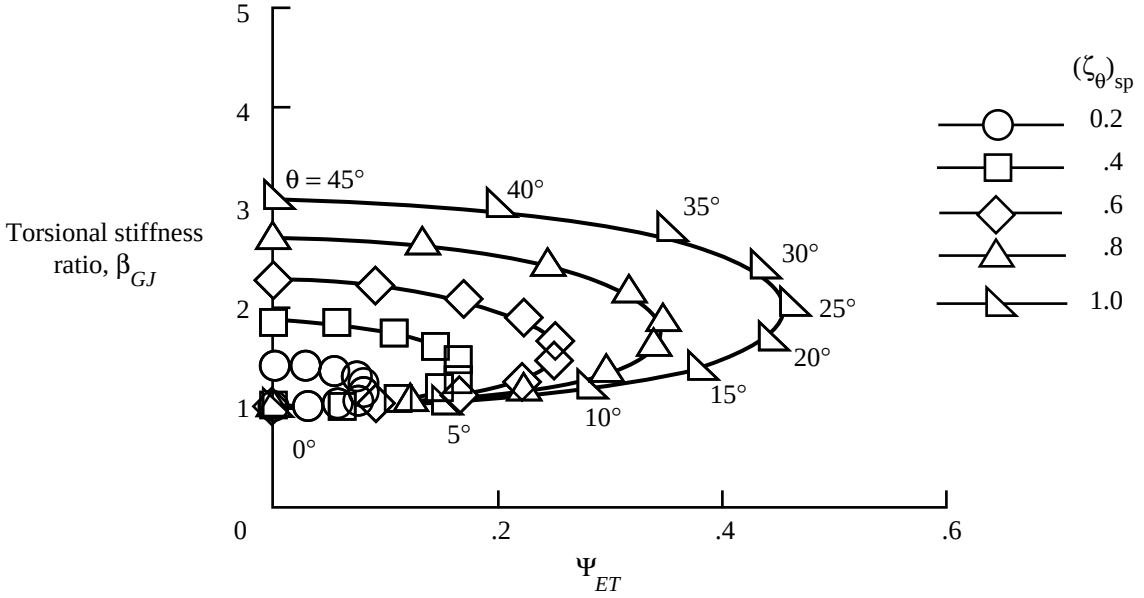

Figure 51. Torsional stiffness ratio as a function of extension-twist coupling parameter for changes in $(\zeta_\theta)_{sp}$ of the baseline 2 blade with antisymmetric laminate construction.

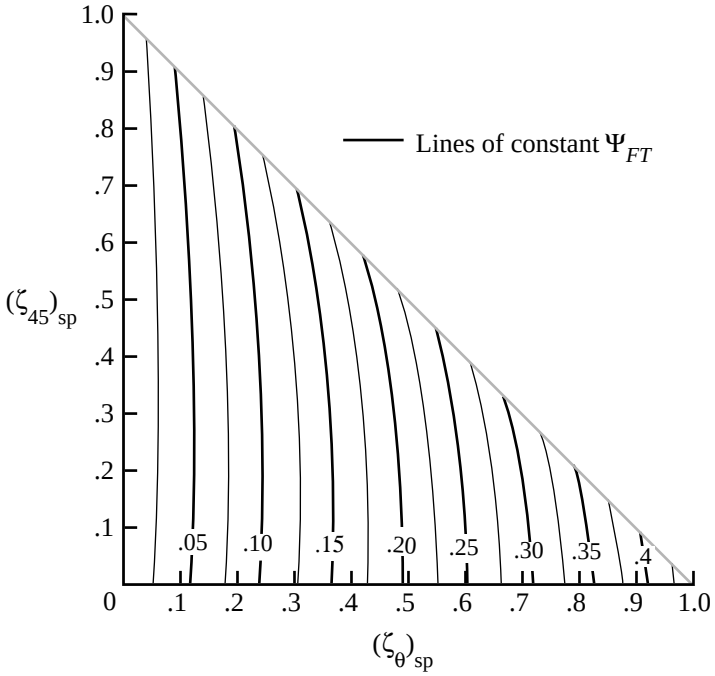

Figure 52. Effect of $(\zeta_\theta)_{sp}$ and $(\zeta_{45})_{sp}$ on flapwise-bending-twist coupling parameter of the baseline 2 blade with symmetric laminate construction.

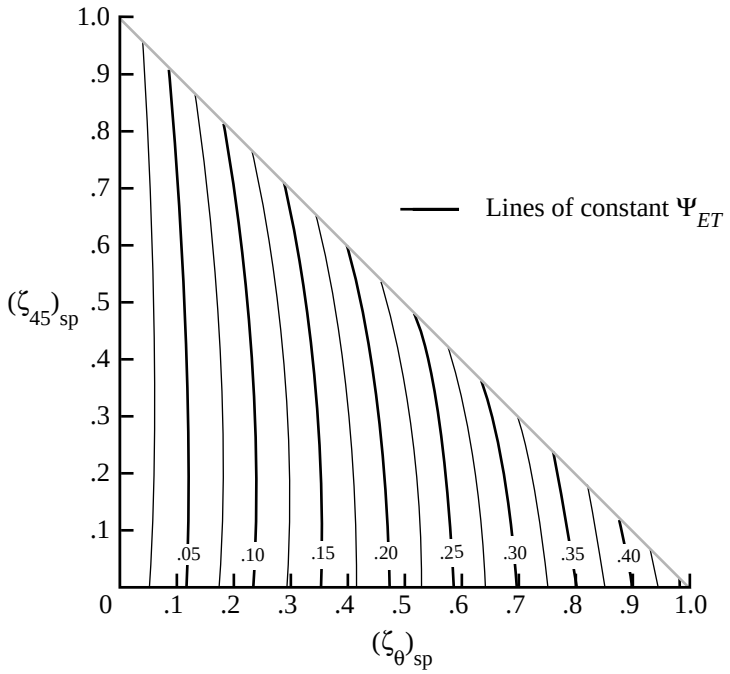

Figure 53. Effect of $(\zeta_\theta)_{\mathrm{sp}}$ and $(\zeta_{45})_{\mathrm{sp}}$ on extension-twist coupling parameter of the baseline 2 blade with antisymmetric laminate construction.

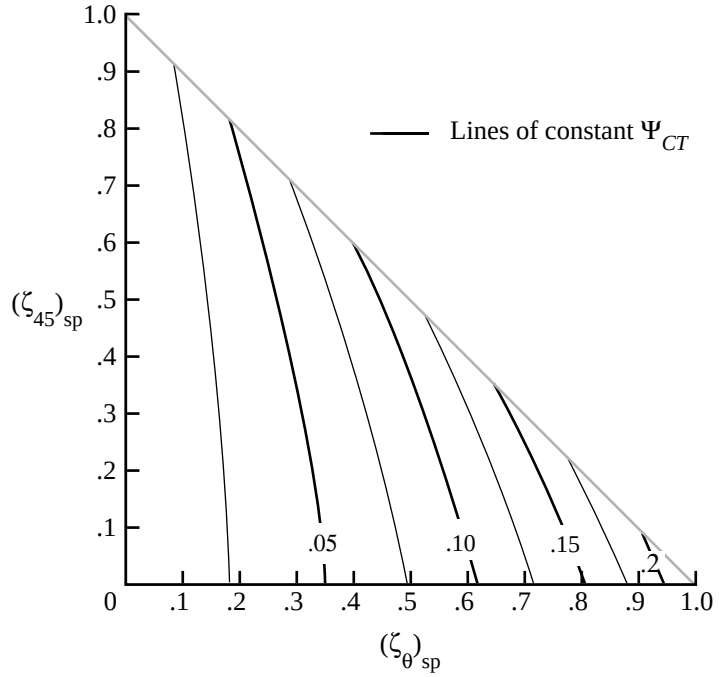

Figure 54. Effect of $(\zeta_\theta)_{\mathrm{sp}}$ and $(\zeta_{45})_{\mathrm{sp}}$ on chordwise-bending-twist coupling parameter of the baseline 2 blade with antisymmetric laminate construction.

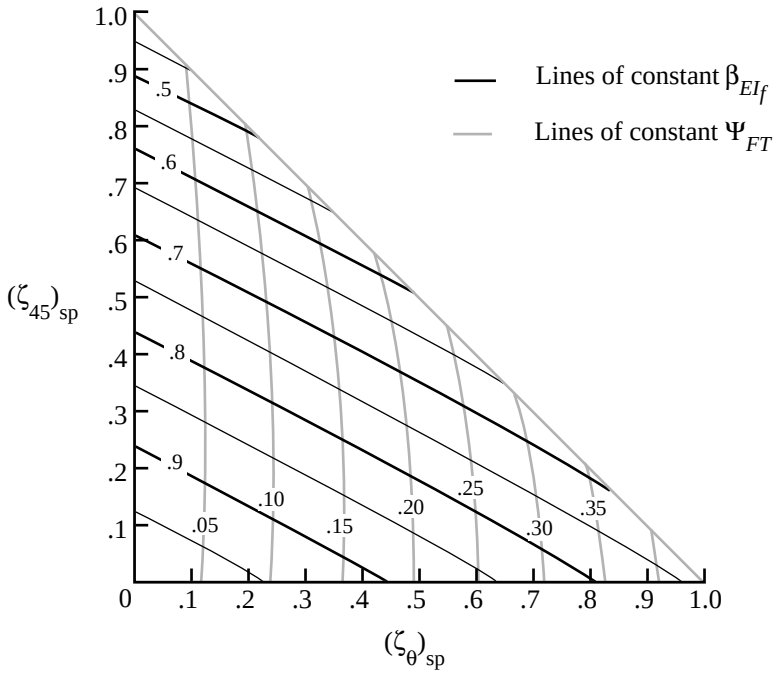

Figure 55. Effect of $(\zeta_{\theta})_{sp}$ and $(\zeta_{45})_{sp}$ on flapwise bending stiffness ratio of the baseline 2 blade with symmetric laminate construction.

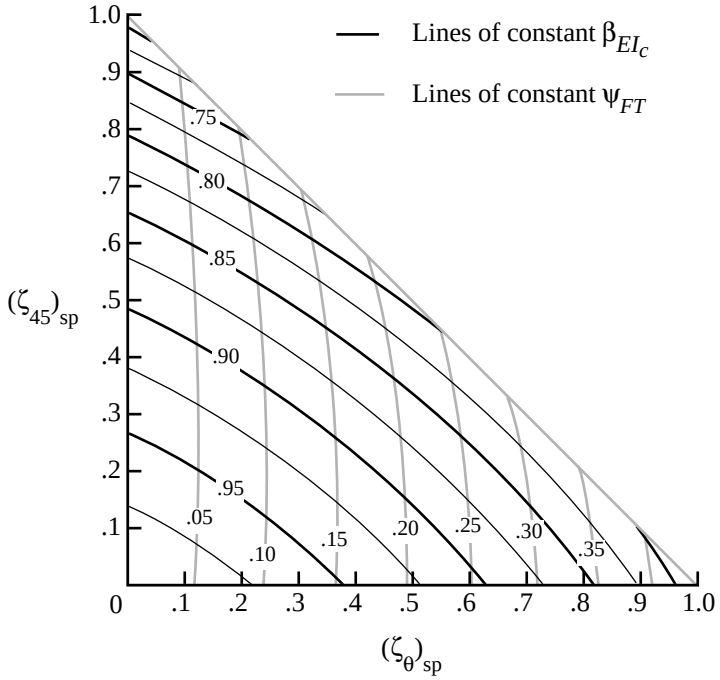

Figure 56. Effect of $(\zeta_{\theta})_{sp}$ and $(\zeta_{45})_{sp}$ on chordwise-bending stiffness ratio of the baseline 2 blade with symmetric laminate construction.

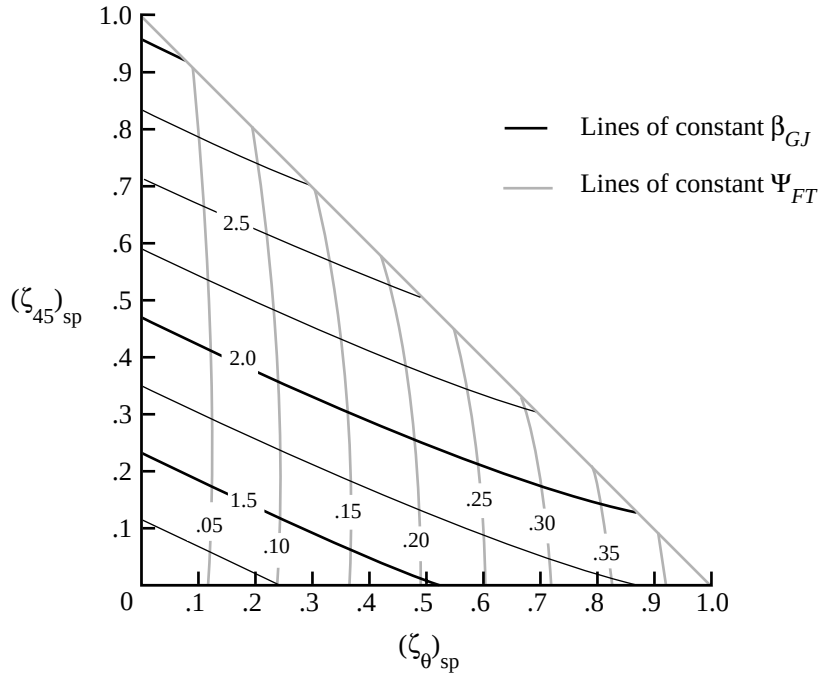

Figure 57. Effect of $(\zeta_\theta)_{\mathrm{sp}}$ and $(\zeta_{45})_{\mathrm{sp}}$ on torsional stiffness ratio of the baseline 2 blade with symmetric laminate construction.

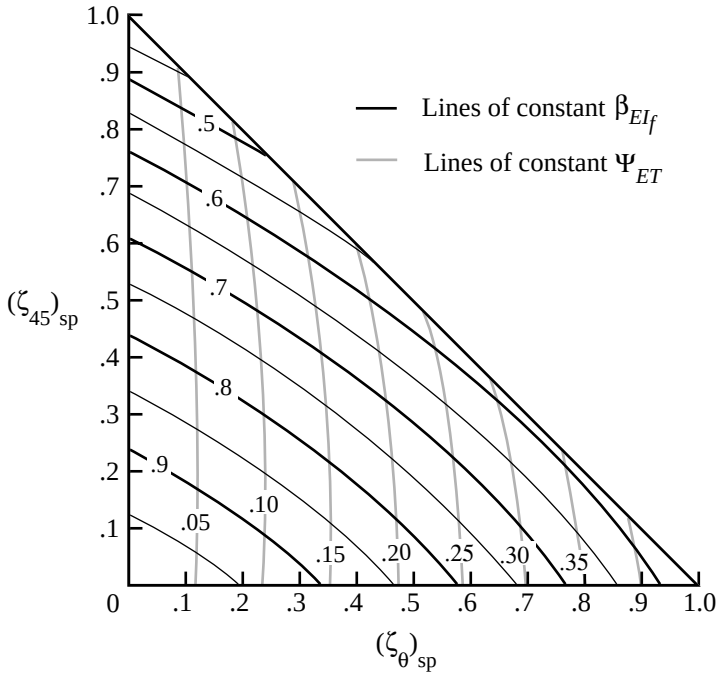

Figure 58. Effect of $(\zeta_\theta)_{\mathrm{sp}}$ and $(\zeta_{45})_{\mathrm{sp}}$ on flapwise bending stiffness ratio of the baseline 2 blade with antisymmetric laminate construction.

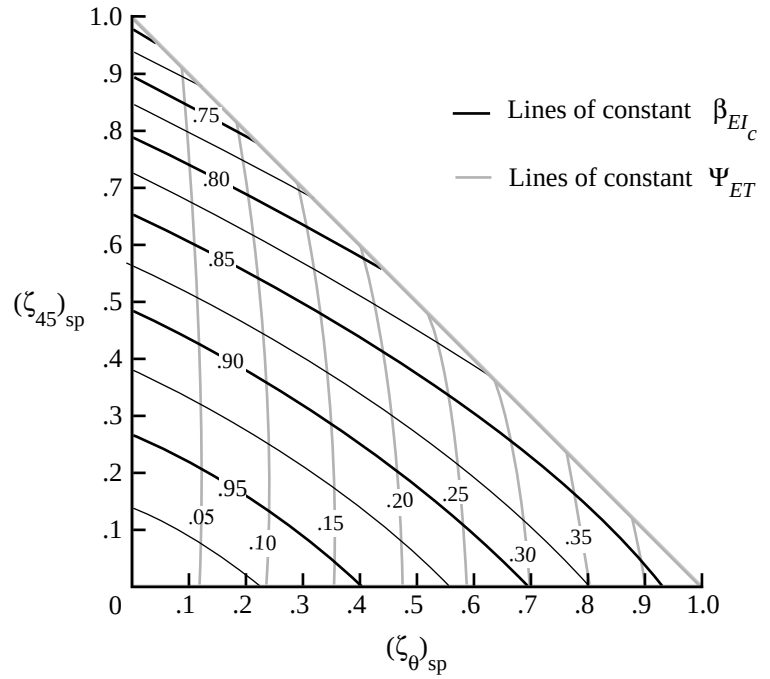

Figure 59. Effect of $(\zeta_\theta)_{\mathrm{sp}}$ and $(\zeta_{45})_{\mathrm{sp}}$ on chordwise-bending stiffness ratio of the baseline 2 blade with antisymmetric laminate construction.

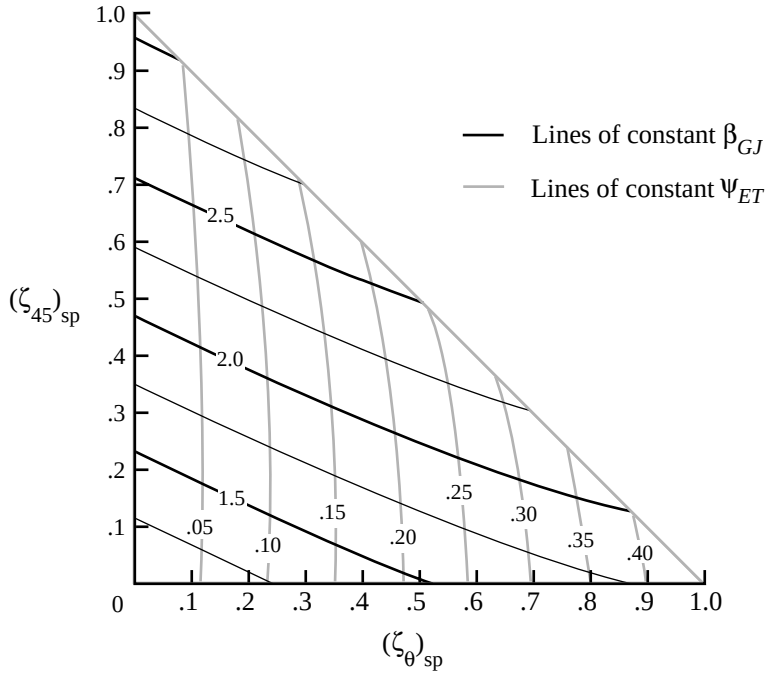

Figure 60. Effect of $(\zeta_\theta)_{\mathrm{sp}}$ and $(\zeta_{45})_{\mathrm{sp}}$ on torsional stiffness ratio of the baseline 2 blade with antisymmetric laminate construction.

REPORT DOCUMENTATION PAGE

Form Approved
OMB No. 0704-0188

1. AGENCY USE ONLY *(Leave blank)*

2. REPORT DATE
April 1997

3. REPORT TYPE AND DATES COVERED
Technical Paper

4. TITLE AND SUBTITLE
Stiffness Characteristics of Composite Rotor Blades With Elastic Couplings

5. FUNDING NUMBERS
WU 505-63-36-02

PR A5008

6. AUTHOR(S)
David J. Piatak, Mark W. Nixon, and John B. Kosmatka

7. PERFORMING ORGANIZATION NAME(S) AND ADDRESS(ES)
NASA Langley Research Center
Hampton, VA 23681-0001

Vehicle Structures Directorate
U.S. Army Research Laboratory
NASA Langley Research Center
Hampton, VA 23681-0001

8. PERFORMING ORGANIZATION REPORT NUMBER
L-17442

9. SPONSORING/MONITORING AGENCY NAME(S) AND ADDRESS(ES)
National Aeronautics and Space Administration
Washington, DC 20546-0001
and
U.S. Army Research Laboratory
Adelphi, MD 20783-1145

10. SPONSORING/MONITORING AGENCY REPORT NUMBER
NASA TP-3641

ARL-TR-1279

11. SUPPLEMENTARY NOTES
Piatak: Langley Research Center, Hampton, VA; Nixon: Vehicle Structures Directorate, ARL, Langley Research Center, Hampton, VA; Kosmatka: University of California, San Diego, CA.

12a. DISTRIBUTION/AVAILABILITY STATEMENT
Unclassified–Unlimited
Subject Category 05
Availability: NASA CASI (301) 621-0390

12b. DISTRIBUTION CODE

13. ABSTRACT *(Maximum 200 words)*
Recent studies on rotor aeroelastic response and stability have shown the beneficial effects of incorporating elastic couplings in composite rotor blades. However, none of these studies have clearly identified elastic coupling limits and the effects of elastic couplings on classical beam stiffnesses of representative rotor blades. Knowledge of these limits and effects would greatly enhance future aeroelastic studies involving composite rotor blades. The present study addresses these voids and provides a preliminary design database for investigators who may wish to study the effects of elastic couplings on representative blade designs. The results of the present study should provide a basis for estimating the potential benefits associated with incorporating elastic couplings without the need for first designing a blade cross section and then performing a cross-section analysis to obtain the required beam section properties as is customary in the usual one-dimensional beam-type approach.

14. SUBJECT TERMS
Elastic couplings; Composite; Rotor blades

15. NUMBER OF PAGES
45

16. PRICE CODE
A03

17. SECURITY CLASSIFICATION OF REPORT	18. SECURITY CLASSIFICATION OF THIS PAGE	19. SECURITY CLASSIFICATION OF ABSTRACT	20. LIMITATION OF ABSTRACT
Unclassified	Unclassified	Unclassified	